Delft University of Technology

Natural Arc Extinction in Air

Kara Olson

TU Delft

Natural Arc Extinction in Air

by

Kara Olson

to obtain the degree of Master of Science

at the Delft University of Technology,

to be defended publicly on Wednesday June 25, 2025 at 1:00 PM.

Student Number:	5935237	
Thesis Committee:	prof. ir. P. T. M. Vaessen	TU Delft, Thesis Advisor and Chair
	dr. ir. D. van der Born	TU Delft, Daily Supervisor and Core Member
	prof. dr. ir. M. Popov	TU Delft, Core Member
	ir. C. S. Engelbrecht	TU Delft and DNV, External Advisor

Cover Image: C.S. Engelbrecht

An electronic version of this thesis is available at `http://repository.tudelft.nl/`.

TU Delft

Abstract

Many overhead transmission lines in the Netherlands are multi-circuited; when one circuit is de-energized for maintenance, the other remains energized. The energy transition necessitates more transmission line reinforcements and heavier loading of existing lines to meet the increasing power demand, consequently increasing the need for additional linework. The energized circuit induces a voltage (EMF) and current in the circuit being worked on. As a further safety measure, line workers utilize a portable earthing device (PED) that is attached to the de-energized circuit's conductors. The induced voltage and current in the circuit can cause arcs up to half a meter long when attaching or detaching the PED, posing a serious threat to workers' safety. There are no active mechanisms in place to stop the arc, so it must naturally extinguish in air.

This thesis aims to model and characterize naturally extinguishing arcs in air. There is little available literature on this topic, which primarily consists of models for static free-burning arcs in air. There are two key objectives in this research: (1) develop a mathematical expression describing the behaviors of naturally extinguishing arcs in air and (2) use the derived expression to produce an arc model simulation verifying the expression's validity and accuracy. The provided test data, including arc videos and oscilloscope data, encompassed arcs under various testing conditions and utilized a test setup that mimicked the arcing environment of a PED being detached from a conductor. The arc distances were approximated using MATLAB image processing techniques due to the videos' poor quality in showcasing the arc distances. These approximated arc distances and oscilloscope data were examined and manipulated to develop an overarching arc expression that represents the resistance-current relationship evident in free-burning arcs in air. Two expressions were derived for comparison: a logarithmic expression and a power law expression. These expressions were implemented in two separate ATP-EMTP software models that each utilized a MODELS-language module to represent the arc for simulation.

The resulting resistance and voltage-current characteristics of the two models were compared against the original test data. The power law expression was found to be the more accurate of the two models. Different testing conditions were then applied to the arc model to identify their natural arc extinction distances, which were also compared against the original test data. The results establish that the power law expression arc model sufficiently predicts the natural arc extinction distance. These predictions can be improved in the future with more precise test data. This thesis's research fills a gap in the existing literature on modeling natural arc extinction in air. The findings of this research can influence future safety procedures for the line workers who experience these arcs. Furthermore, the results of the arc model for PED removal can potentially be expanded to describe the arcing behavior of disconnectors during bus transfer assessment, leading to a greater understanding of disconnectors and providing a deeper insight into their application and test result interpretations.

Acknowledgements

I would like to express my sincerest thanks to all who have contributed to the completion of this thesis with their support and guidance. Firstly, I would like to thank my thesis advisor, Peter Vaessen, and daily supervisor, Dennis van der Born, for their continued support and advice on pursuing this academic endeavor. I would also like to especially thank my external advisor, Christiaan Engelbrecht, for his invaluable support, encouragement, and guiding advice throughout my thesis, whose comments, suggestions, and knowledge have stimulated and shaped my research and problem-solving capabilities.

From the bottom of my heart, I would like to express my deepest gratitude to my beloved parents and twin sister for their steadfast, unconditional love, support, and guidance. To my mom, thank you for being my voice of reason and my rock to turn to in everything I do. A special thank you to my dad, whose love and light inspire me every day and for our endless conversations about my thesis, electricity, and everything in between. All of my endeavors are only possible because of the three of you. Finally, I would like to thank any friends and colleagues who have either indirectly or directly influenced or contributed to the completion of this thesis with their insights and support.

Contents

List of Figures

List of Tables

Chapter 1

Introduction

1.1 Arcing in Portable Earthing Devices (PEDs) due to Inductive Coupling from Parallel Energized Circuits

In the Netherlands, most overhead lines are multi-circuited; more than one high-voltage or extra-high-voltage circuit is typically strung along the same towers in parallel. This multi-circuited overhead line approach is common in the Netherlands and abroad due to spatial constraints [1]. During maintenance, one circuit is taken out of service to perform work while the other remains in service. In these instances, the energized circuit is more heavily loaded to make up for the lost power flow in the circuit being worked on. The more heavily loaded line results in a higher current flowing through the circuit, which, in turn, increases both the electromagnetic coupling effects in the circuit and the induced voltage and current in the grounded circuit being worked on. Inductive coupling is dominant in the earthed circuit being worked on [1]. Inductive coupling occurs when the high current flowing in the energized circuit establishes a large magnetic flux that also encompasses the de-energized circuit due to the circuits' proximity to one another. The result of this inductive coupling is an induced voltage (EMF) and current in the de-energized circuit. An illustration of inductive coupling in a parallel circuit is shown in Figure 1.1.

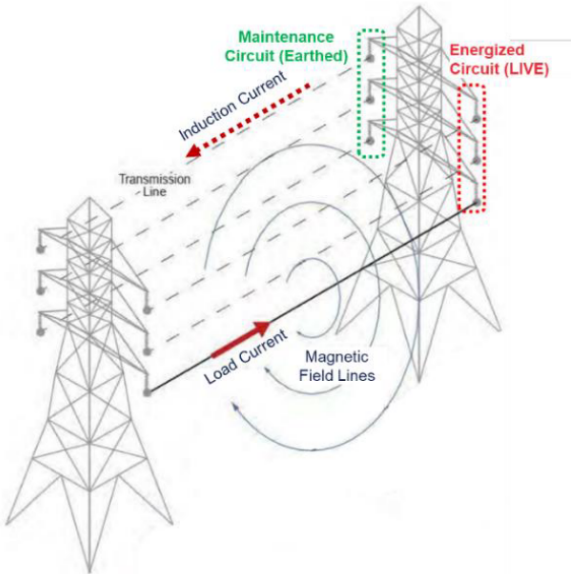

Figure 1.1: Induced Parallel Circuit, from [1]

Portable earthing devices (PEDs) are utilized at the work site to ensure the workers' safety when performing maintenance work on a de-energized circuit. PEDs serve to ground, or discharge, any potential voltage or current that may exist in the de-energized circuit. This grounding, or earthing, is done by installing the PED—which comprises a long earthing cable and clamps at the ends—between the conductors to be worked on and the supporting tower or structure as well as on the adjacent towers on either side of the work tower, which is known as bracket earthing [1]. Two examples of a PED are displayed in Figure 1.2.

(a) Portable Earthing Device with Earthing Wire, from C.S. Engelbrecht

(b) Portable Earthing Device, from [1]

Figure 1.2: Examples of Portable Earthing Devices (PEDs)

Due to the induced voltage and current that may be present in the de-energized circuit, arcs can occur between the PED and line conductor when connecting or disconnecting PEDs. There are no active mechanisms in place to limit the arc, so the workers must rely on the arc extinguishing naturally in air. In cases where there are large induction effects, natural extinction of the arc may no longer occur, presenting a huge safety concern for workers.

1.2 The Significance of Naturally Extinguishing Arcs in Air

The study and analysis performed in [1] form much of the reasoning behind why the research of this thesis is pertinent and presents the objective of creating a mathematical model and simulation for natural arc extinction in air. Recognizing the impact a naturally extinguishing arc in air (caused by induced coupling in parallel circuits) has on the safety of workers and the equipment being worked on is imperative in promoting safer working conditions and more robust guidelines on installing and removing PEDs as well as dealing with the potential arcing during the process. The behaviors of an arc in air and their influence on the voltage, current, and resistance of the arc play a significant role in creating an accurate, informative arc model. Developing an accurate, predictive model of natural arc extinction in air can lead to a better understanding of arcs in air and whether PEDs can safely be removed.

In this research, as explained in [1], natural arc extinction in air refers to the extinction of an arc when PEDs are removed. The "natural arc extinguishing distance" describes the distance between the two electrodes where the natural arc extinction occurs [1]. Similarly, the arc distance—for this research—is defined as the distance between the two electrodes at any given point in time during the arc's duration. This natural arc extinguishing distance is contrary to the typical arc length and reach utilized in arc models and calculations. The arc distance, arc length, and arc reach are illustrated in Figure 1.3.

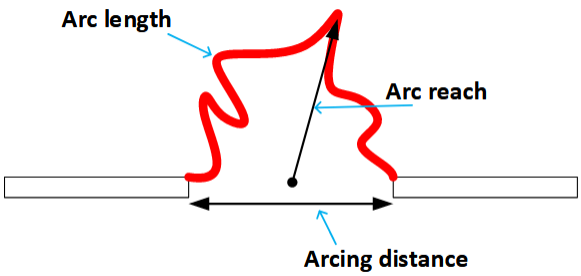

Figure 1.3: Arc Distance, from [1]

The natural arc extinction distance depends on the current being interrupted and the voltage that appears between the electrodes after the arc extinguishes. At present, there is little information available on how the natural arc extinguishing distance relates to the current and open-circuit voltage. However, an empirical relationship has been proposed based on the limited laboratory test results in [1]. The representative arc model presented in this thesis builds upon this existing information to provide a more quantitative description for understanding natural arc extinction in air and aims to augment laboratory-based arc testing by simplifying the design

process and providing deeper insights into the studied arcs. A better understanding of natural arc extinction in atmospheric air and the natural extinguishing distance is paramount to maintaining workers' safety during overhead line maintenance. Furthermore, the findings in this research can be applied to other grounding devices, such as temporary grounding devices, in addition to PEDs. This research will also work to better inform safety procedures and protocols for working on overhead lines.

1.3 Objectives

There are two primary objectives of this thesis research, which are described as follows:

- A mathematical expression describing natural arc extinction in air will be developed by extracting the test data from tests conducted at Damstra Laboratory in Hengelo and initiated for the research done in [1].

- An ATP-EMTP model will be developed to simulate and corroborate the findings from the mathematical expression describing natural arc extinction in air. The findings from [1] and [2] are used as base references for determining the accuracy of the model simulations.

1.4 Project Overview

A literature review is conducted to examine the relationships present in arcs in atmospheric air and to determine the most relevant type of existing arc model as a reference for developing a new arc model on natural arc extinction in air that applies to the removal of PEDs on transmission lines.

Laboratory testing was performed for DNV Netherlands in March 2023 to obtain a better understanding of the arc behavior when removing PEDs. Data in the form of arc videos and voltage and current oscilloscopes were recorded under 26 different testing conditions by varying the voltage, current, and speed of a movable electrode (representing the speed at which the PED is removed). The test data from each of the provided arc videos and corresponding oscilloscopes are extracted and filtered using MATLAB. The arc distances throughout the duration of the arc are determined through image processing of the videos.

Empirical relationships between the arc voltage, current, and resistance (normalized by arc distance) are then analyzed to find two trendlines representative of the data for each respective video: one expression as a power law function and the other as a logarithmic function. These trendlines for each type of function are then averaged together to obtain the overarching mathematical expressions to describe the PED-related arc behaviors.

These mathematical expressions are implemented in ATP-EMTP simulation models using the MODELS language. Multiple models are made in ATP-EMTP for comparison: a reference model based on the findings in [2], a model based on power law mathematical approximations of data, and a model based on logarithmic mathematical approximations of data. The simulated results are then analyzed to determine

which model is the most accurate and representative of natural arc extinction in air. Finally, the most representative arc model is employed to predict natural arc extinction distances for comparison against the original test data and findings from [1].

1.5 Thesis Overview

This thesis is divided into five chapters, with the first being this introduction. The following chapters are described as follows:

- Chapter 2 is a literature review that examines various types of arc models and determines the most relevant one for modeling natural arc extinction in air. It then goes on to describe the characteristics and expected behaviors of the selected arc model and provides specific modeling examples for reference.

- Chapter 3 describes the test setup utilized during the arc testing for DNV and the methods used for extracting data and calculating the mathematical expressions for natural arc extinction in air. It then goes on to explain how the expressions are implemented in ATP-EMTP software as well as describe the testing processes associated with simulating the model. The chapter then outlines the methods of comparing the resulting data with the original test data.

- Chapter 4 contains the results of the calculations and simulations presented in Chapter 3, analyzing and discussing their relevance in understanding natural arc extinction in air. The results are then compared against those found in [1] to further contextualize this thesis's findings regarding the removal of PEDs.

- Chapter 5 concludes the thesis research by summarizing the research and highlighting its most significant findings. Recommendations are also provided for future work on the topic.

Chapter 2

Literature Review

The successful development of an arc model is dependent on its ability to accurately reflect the nature of the arc being studied. The available literature on arc modeling motivates this thesis's methodology to create a more robust model for natural arc extinction in air. Much of the current literature has focused on arcs in switching, circuit breakers, secondary arcs, and free-burning arcs. While this research is important in understanding the greater picture of arcs and how they work, not all of these arc models may be representative of the specific condition that is the removal of PEDs. It is thus important to analyze, synthesize, and reflect on the existing literature concerning modeling natural arc extinction in air and emphasize the most relevant literature available. This literature review focuses on extracting information necessary for developing an accurate, predictive model for natural arc extinction in air.

This review examines various types of arc models presented in the available literature and determines which model best serves the purposes of this research through analysis and elimination. Literature on the most relevant arc model is then discussed in greater detail. The available literature on arc models has primarily consisted of the following types:

- Circuit Breakers
- Air-Break Disconnector Switches
- Secondary Arcs
- Free-Burning Arcs

2.1 Circuit Breakers

Circuit breakers form the basis of much of the existing literature on electric arcs and are used for current interruption in the case of a fault occurring in a system. An arc is established in the gap between the contacts of a circuit breaker while the current is still flowing [3]. The purpose of the circuit breaker is to extinguish the arc occurring in the circuit by halting the current flow in the circuit. The fault arc found in circuit breakers is considered a "confined" arc with its shorter length (in the order of a few centimeters) and more predictable behavior. For this research, only air circuit breakers are considered since it is also the medium in which the arcs from PED removal occur; other types of circuit breakers utilize gas, oil, or a vacuum

as their medium for current interruption, which is not relevant to the topic of this research. The arc in an air-blast circuit breaker is cooled and extinguished by a blast of high pressure air [3][4][5][6]. Circuit breaker arc elongation in air can be modeled as in Figure 2.1 with the arc voltage across the gap in the circuit breaker proportional to the arc length.

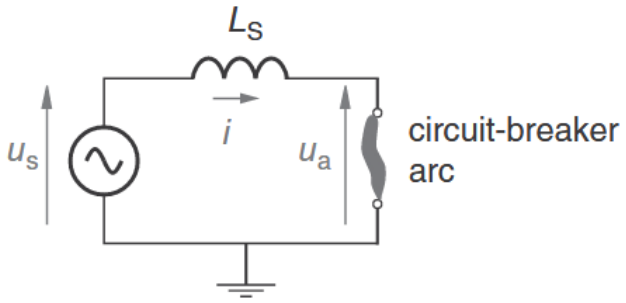

Figure 2.1: Circuit Breaker Arc Model Circuit, from [3]

As the arc length and voltage increase, the arc current decreases to a point at which the arc is extinguished, interrupting the current in the circuit. Air circuit breakers provide a well-studied, predictable arc model for understanding the basis of arc formation and extinguishing.

Despite the extensive research on arcs in circuit breakers, the behaviors dominating the arc in a circuit breaker are fundamentally different from those of an arc resulting from PED removal. The currents and recovery voltages that a circuit breaker must break are significantly higher than those in naturally extinguishing arcs in air due to the removal of a PED (up to approximately 800 kV and 100 kA for circuit breakers compared to 2.4 kV and 0.8 kA for PED removal [1][3][5][7]). Although the voltage, current, and resistance (conductance) relationships of an arc in an air circuit breaker act similarly to those from PED removal, the confined behavior of arcs in circuit breakers is juxtaposed against the random, unconfined behavior evident in the arcs from PED removal. The unconfined nature of arcs from PED removal causes their distance and time-to-extinguish to be significantly longer and more unpredictable than those modeled in circuit breakers. The conditions in which an arc in a circuit breaker takes place are also different from the conditions that ignite an arc when removing a PED; circuit breakers are utilized in energized circuits to de-energize the part of the system in which the fault occurs, whereas arcs from PED removal are inductively sourced and occur in a grounded circuit. Additionally, air circuit breakers at atmospheric pressure may only be used in low- and medium-voltage applications (up to 15 kV [8]) due to atmospheric air's low interruption capabilities [3][5]. Air-blast circuit breakers utilize pressurized air to increase arc voltage, thus minimizing the arc current for interruption [5]. While arcs from the removal of a PED occur in air, no such pressurized air mechanism is employed, further discrediting circuit breaker models as a logical basis for this research's arc models since the atmospheric air circuit breakers are confined to such specific scenarios and would not be entirely representative of the conditions for arcs occurring from disconnecting PEDs.

2.2 Air-Break Disconnector Switches

Air-break disconnector switches are primarily used for current interruption in atmospheric air to isolate a portion of the system under no load conditions [9]. The arc in an air-break disconnecting switch behaves as a free-burning arc, with similar extinction criteria and arc characteristics [10]. [9] also maintained that successful current interruption depends on an established minimum gap distance instead of a critical arc distance (as is the case for arcs from PED removal). Air-break disconnector switches operate by opening the disconnector switch manually or via a motor, and an arc forms as the contacts of the switch separate. The arc grows as the gap between the contacts in the disconnector switch increases until arc extinction is achieved. An example of an opened air-break disconnector switch is shown in Figure 2.2.

Figure 2.2: Example of an Air-Break Disconnector Switch, from HAPAM B.V., as cited by [9]

The nature of the arc and its parameters, such as arc length, minimum gap distance, and extinction time, is dependent upon the type of current flowing through the system: capacitive current, transformer magnetizing current, and loop currents [9].

Much of the existing literature on air-break disconnector switches has focused on capacitive current interruption, which [4] claimed more closely resembles secondary arcing (discussed in section 2.3). The recovery voltage—the voltage that appears between the contacts after the arc is interrupted—is much higher than in the case of arcs from PED removal (in the range of tens and hundreds of kilovolts for disconnector switches [9]), which results in restrikes. These restrikes are the determining factor in whether or not the arc in the air-break disconnector switch will extinguish; this restrike behavior is not present when disconnecting PEDs.

2.3 Secondary Arcs

Secondary arcs exhibit seemingly similar behaviors to arcs from PED removal due to the influence of coupling and their natural extinction in air, which suggests it is a plausible candidate for further development of an arc model for natural arc extinction in air. Secondary arcs materialize in a faulted system after a primary arc (typically arising from a single-phase fault when single-phase closing is applied) across a circuit breaker has been extinguished. A secondary arc occurs when the primary arc is extinguished and enough of its ionized channel remains in the air. The capacitive coupling in the surrounding live phases provides enough energy to drive the secondary arc after the primary arc has been extinguished [11]. The capacitively coupled source of secondary arcs makes them unique compared to the other arcs examined in this literature review because the coupled source influences the arc current and thus the arc characteristic. Secondary arcs also extinguish naturally in air [11]. The coupled source and natural arc extinction in air are important commonalities between secondary arcs and the arcs occurring from PED removal. These influences play a significant role in the behaviors and characteristics of the arcs that will, in turn, influence the arc model.

Despite similar behaviors and characteristics between secondary arcs and arcs from PED removal, their fundamental differences suggest secondary arcs are less relevant when developing the model for natural arc extinction in air. An arc resulting from disconnecting a PED is mostly driven by inductive current, and any present capacitance is negligible. Secondary arcs also differ from arcs from PED removal due to their longer arcing distance. The capacitive coupling in secondary arcs produces a different arc current characteristic and recovery voltage than that of an inductively coupled arc. These differences are evidenced in the comparison of free-burning and secondary arc characteristics, as shown in Figure 2.3, from [9]. [9] utilized the findings from studies by Gross [12] and Anjo [13], respectively.

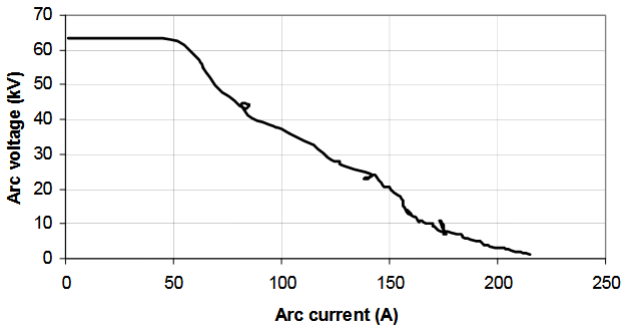

(a) Free-Burning Arc U-I Characteristic, from [12] as cited by [9]

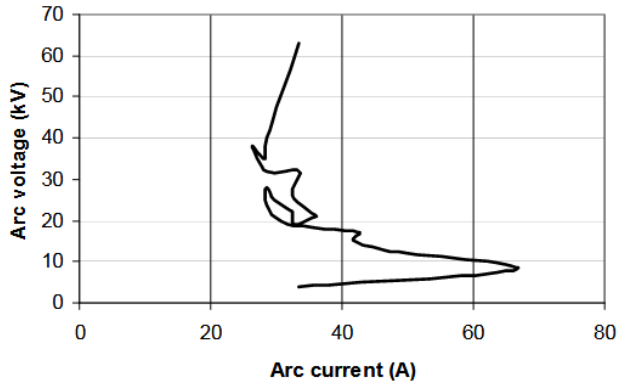

(b) Secondary Arc U-I Characteristic, from [13] as cited by [9]

Figure 2.3: Free-Burning and Secondary Arc U-I Characteristic Comparison

From the U-I characteristics Figure 2.3 displays, the influence of capacitive coupling becomes more apparent. The irregular characteristics and erratic behavior present in secondary arcs do not resemble behaviors found in the laboratory tests in [7] that this thesis looks to model, and therefore disqualify the secondary arc from being the best candidate for modeling natural arc extinction in air.

2.4 Free-Burning Arcs

Free-burning arcs in air are unconstrained and thus exhibit random, irregular behaviors and patterns compared to "confined" arcs, such as those in circuit breakers. Free-burning arcs in air may occur under various circumstances. However, the principle of how they work remains the same: as two electrodes begin to separate, a highly conductive plasma channel forms between them, allowing current to flow through the ionized medium—in this research's case, atmospheric air. This plasma channel between the electrodes, and with current running through it, is the electric arc in air [3]. Because there is no mechanism in place to stop the arc, it continues to propagate in the air as the electrodes continue to separate, only extinguishing when the arc has reached a sufficient distance that causes the arc current to remain at 0 A. As the distance between electrodes increases, the arc voltage also increases. Arc elongation—or the growth of the arc distance—occurs as the voltage continues to increase due to the arc distance and arc voltage being proportional to one another. The arc completely extinguishes when a certain distance threshold between the electrodes is reached [14]. Unconstrained, complex behaviors dominate free-burning arcs in air, making them a unique case in the study of electric arcs.

Free-burning arcs and their unconfined behavior present the best basis for developing a model of arcs resulting from disconnecting PEDs. Like with the arcs occurring due to PED removal, there is no mechanism in place to extinguish free-burning arcs in air. Therefore, the arc extinguishes naturally in air according to the conditions that are outlined in section 2.5. This natural arc extinction in air is contrary to many of the other types of electric arcs explored in much of the existing literature on arc modeling, such as those discussed in the above sections. The unconstrained, random behavior of free-burning arcs in air reflects that of the arcs from PED removal that arise when disconnecting the device from the de-energized circuit with an induc-

tively coupled source supplying the current. The building of an arc model for arcs resulting from disconnecting PEDs will therefore be based on the models developed in pre-existing literature on free-burning arcs in air. The irregular, unconstrained behaviors of free-burning arcs in air best reflect the behaviors seen in arcs from PED removal.

2.5 Arc Characteristics of Free-Burning Arcs

The arc characteristics of a free-burning arc in air are influenced by the arc's irregular, unconfined nature. The arc characteristic is nonlinear, which causes shape distortion in the arc voltage. The arc U-I characteristics in [14] are consistent with the findings of [2], which maintained that electric arcs are highly variable, complex, and nonlinear. Therefore, the arc distance is also highly variable and nonlinear, and the arc voltage is greatly influenced by this arc distance [2]. The arc channel consists of resistive plasma, and resistance is proportional to the arc's distance; thus, the arc voltage is proportional to the arc distance. Inversely, the arc voltage (and therefore arc resistance) increases with decreasing current [3]. The nonlinear, variable behavior of a free-burning arc in air has a profound impact on the arc's voltage, current, and resistance.

2.5.1 U-I Characteristics and Resistance

The U-I characteristics and resistance of free-burning arcs in air are influenced by their long, non-conforming behaviors. Arc power steadily increases as the arc resistance increases and the arc current decreases. The arc extinguishes at the collapse of the power input. Partial arc collapse can also occur before total arc extinction [9]. However, this research focuses primarily on reaching total arc extinction as a result of arc elongation. The arc voltage and current are inversely proportional to one another, as demonstrated by the findings of Gross [12] in Figure 2.6 and discussed in [9].

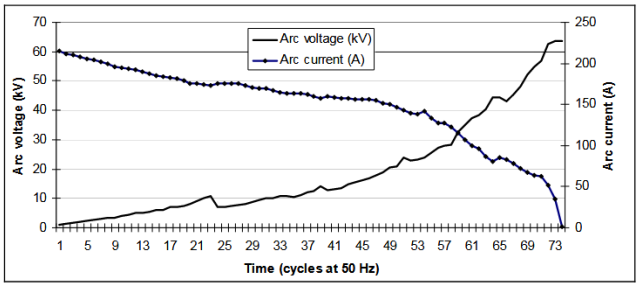

Figure 2.4: Free-Burning Arc in Air Arc Current and Voltage, from [12] as cited by [9]

This inverse voltage-current relationship results in a hysteresis loop-like shape in the U-I characteristic curve, such as in Figure 2.5, further emphasizing the nonlinear nature of the free-burning arc in air.

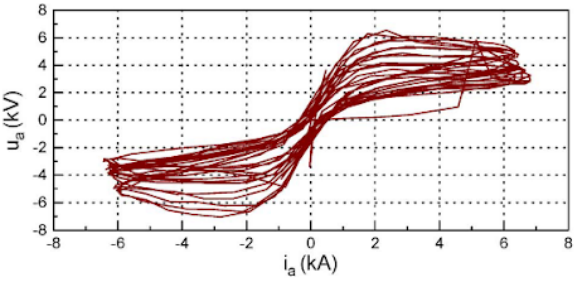

Figure 2.5: Free-Burning Arc in Air Test Results U-I Characteristic, from [2]

The resistive nature of the free-burning arc in air is further supported by the modeling of the arc voltage and currents in Figure 2.6, where they are in-phase with one another.

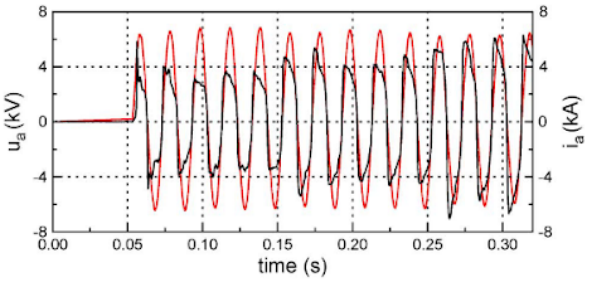

Figure 2.6: Free-Burning Arc in Air Test Results Arc Current and Voltage, from [2]

Arc resistance is found by simply using Ohm's law [2]:

$$r_a(t) = \frac{v_a(t)}{i_a(t)} \quad [\Omega] \tag{2.1}$$

The arc resistance's expected behavior is thus dependent on both voltage and current; the arc resistance is proportional to the arc voltage and inversely proportional to the arc current. In Figure 2.7, the resistance increases significantly at every instance the arc current approaches a zero-crossing, which occurs every half-cycle.

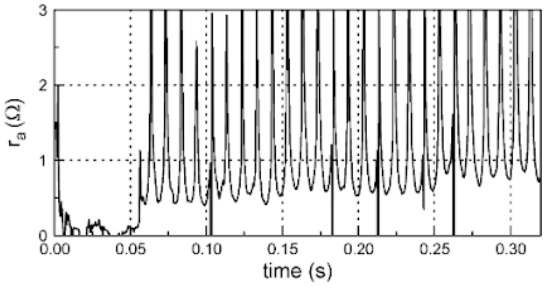

Figure 2.7: Free-Burning Arc in Air Test Results Arc Resistance, from [2]

The arc characteristics and relationships found in free-burning arcs in air are paramount to developing a successful arc model, and these characteristics are directly intertwined with the complex nature of the free-burning arcs.

2.6 Model Expected Outcome

The modeling of a free-burning arc in air has been discussed extensively in several publications by Terzija et al. ([2] [15] [16] [17] [18] [19]) and in [11]. The simplified ATP-EMTP circuit models, shown in Figure 2.8, were similar in these works, with the arc being modeled by the MODELS component connected to a variable resistor (Type-91 resistor in ATP-EMTP software), which represents the changing arc resistance over time.

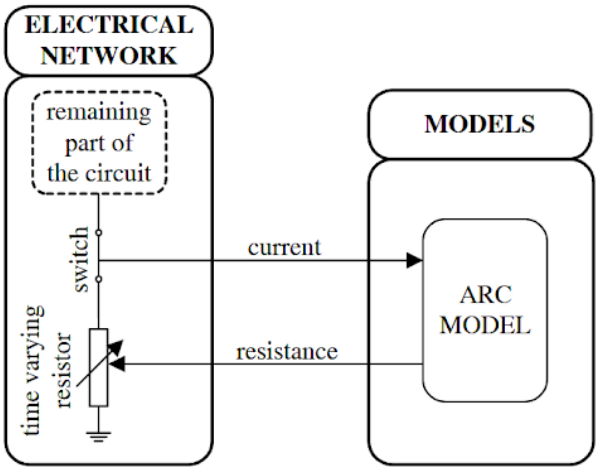

(a) Free-Burning Arc Model Circuit, from [11]

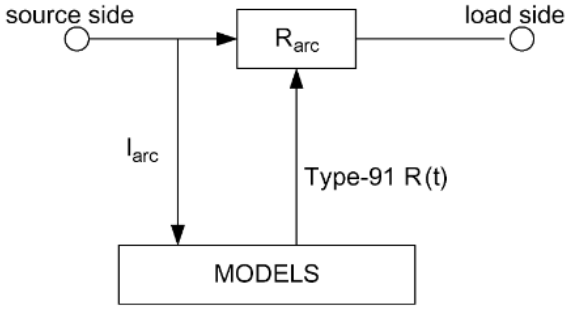

(b) Free-Burning Arc Model Circuit, from [2]

Figure 2.8: Free-Burning Arc Model Circuits

The modeled arc resistances, voltages, and currents for this research should accurately reflect the testing data presented in section 2.5. The simulated U-I characteristic curves and arc resistances from both the Terzija et al. model and [11], shown in Figure 2.9, demonstrate that both models accurately simulated the arc behaviors found in real-life testing scenarios.

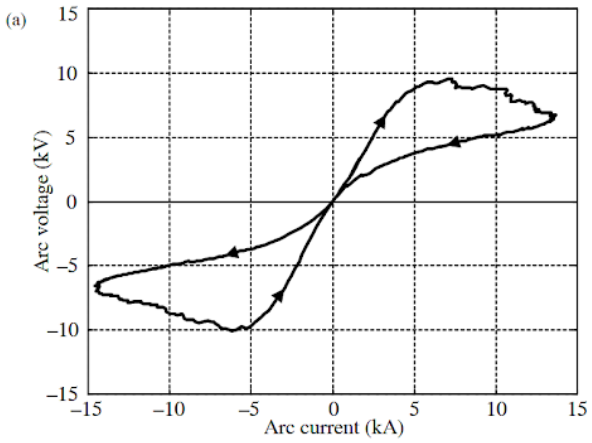

(a) Simulated Free-Burning Arc U-I Characteristic, from [11]

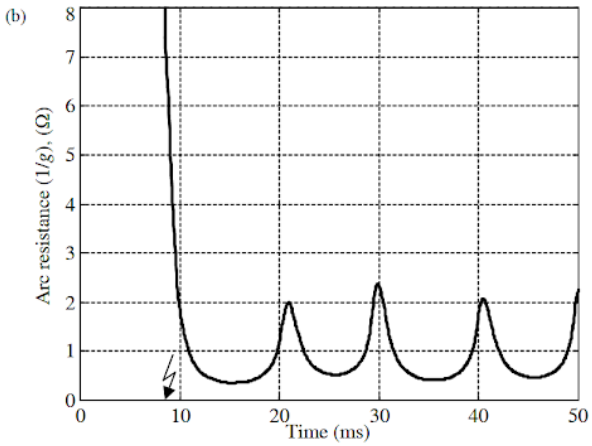

(b) Simulated Free-Burning Arc Resistance, from [11]

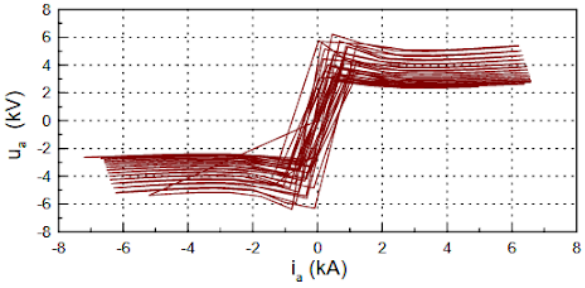

(c) Simulated Free-Burning Arc U-I Characteristic, from [15]

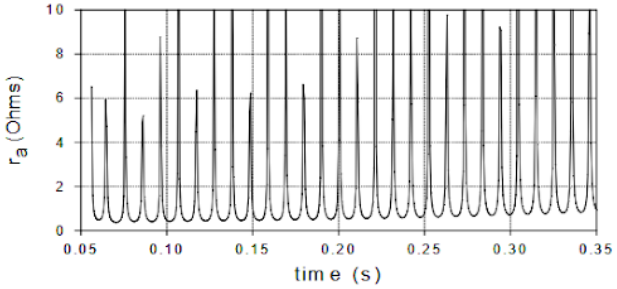

(d) Simulated Free-Burning Arc Resistance, from [15]

Figure 2.9: Simulated Free-Burning Arc U-I Characteristics and Arc Resistances

While both models from [2] and [11] accurately simulated free-burning arcs in air, [2] established an ATP-EMTP MODELS-language-based static model of a free-burning arc with elongation and provided the MODELS-language code for that model. Due to its more extensive descriptions and explanations, this model forms the basis of ATP-EMTP modeling in this research, with the addition of varying arc distances. The free-burning arc models detailed in the works by Terzija et al. and [11] represent accurate simulations relating to the natural arc extinction in air this thesis researches. The accuracy of these Terzija et al. papers is validated by the signal waveshapes of this research's test data [7] and the findings in [4][9][14].

2.7 Conclusions

This literature review aims to analyze the existing literature on circuit breaker arcs, air-break disconnector switch arcs, secondary arcs, and free-burning arcs in air, narrowing down which of these forms the best basis for developing a model on natural arc extinction in air. The arcs occurring as a result of removing PEDs have unique characteristics that must be reflected in their simulations. There does not currently exist much literature on arc modeling of natural arc extinction in air. However, similar models may be consulted when developing a model for natural arc extinction in air to best encompass the arc's behavior for the scenario outlined in this research. This literature review argues that free-burning arcs in air provide the best basis for developing a model on natural arc extinction in air due to PED removal. Furthermore, the behaviors and arc characteristics of free-burning arcs in air are discussed to better understand the expected behaviors of arcs from PED removal. The ATP-EMTP model that will be referenced throughout the remainder of this thesis is presented, and its results are compared against the expected results of free-burning arcs in air as found through real-life testing. The results of this literature review will then be applied to the arcs from PED removal that this thesis proposes to model.

Chapter 3

Methodology

The following chapter outlines the methods utilized to arrive at this research's final results. First, the test data and experimental setup used to acquire that data are described. Next, the test data are extracted from the videos and text files provided for further inspection and manipulation using Excel and MATLAB. Trendlines are created to establish an overall approximation of the data. The ATP-EMTP models employing these trendlines are developed to simulate the original test data. These models contain the information for analysis and comparison in the results and discussion chapter. It is imperative to accurately extract and simulate the test data that recreates the conditions for a naturally extinguishing arc in air from PED removal, which leads to a detailed reference expression and model.

3.1 Test Setup/Data

The tests and test data received for analysis in this thesis were conducted for DNV Netherlands at Damstra Laboratory in Hengelo, the Netherlands, in March 2023 [7]. The test data consisted of 26 high-speed videos and corresponding voltage and current oscilloscope data (given as text files) for different arc testing conditions. These conditions are outlined in Table 3.1. The test number corresponds to the video and oscilloscope file labels given for each test when the data were received. The test numbers omitted in the table either had no load attached, and thus no current running through the circuit, or were meant to check the prospective current (and no arc occurred). These tests were not used in this research because they did not contain any arc information. Therefore, of the 26 testing scenarios provided, 21 contained useful data for further inspection and analysis.

Test Number	**Applied Voltage** [V_{rms}]	**Current** [A_{rms}]	**Moving Electrode Speed** [m/s]	**Frame Rate** [fps]
2	244	230	0.8	1000
3	402	434	0.8	1000
4	592	560	0.8	1000
5	790	737	0.8	1000
6	790	730	0.8	1000
7	980	912	0.8	1000
8	980	912	0.8	1000
11	233	258	0.1	500
12	398	376	0.1	500
13	398	376	0.1	500
14	764	733	0.1	500
15	961	917	0.1	500
17	400	197	0.8	500
18	791	380	0.8	500
19	1174	504	0.8	500
20	1174	504	0.8	500
22	1600	534	0.8	500
23	2000	676	0.8	500
24	2400	818	0.8	500
25	2400	818	0.8	500
26	2400	818	0.8	500

Table 3.1: Testing Conditions, from [7]

The test setup consisted of two electrodes in contact that moved away from each other at a 90°angle to simulate the removal of a PED from a transmission line. As shown in Figure 3.1a, electrode A represents the immovable transmission line, and electrode B represents the PED that is being removed. The movable electrode had a separation distance of up to one meter away from the stationary electrode, and a wheel connected to that movable electrode allowed it to move at a constant speed during the testing, 0.8 m/s or 0.1 m/s.

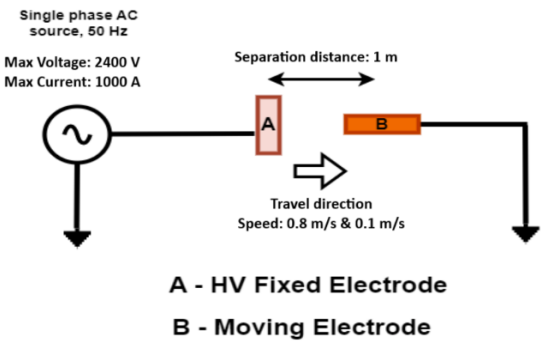

(a) Test Setup Schematic, from [7]

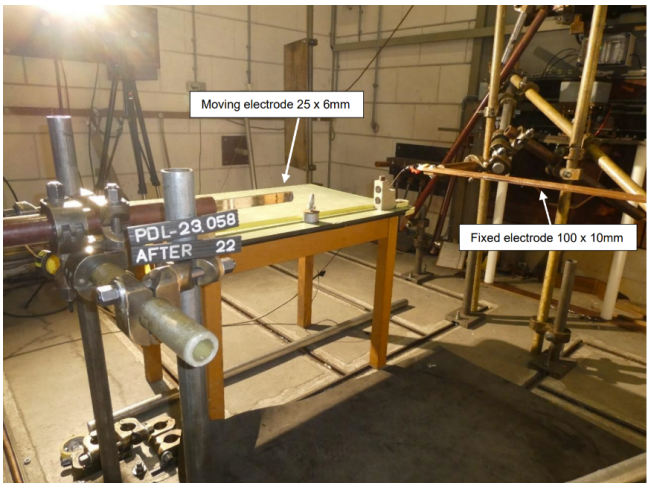

(b) Physical Test Setup, from [7]

Figure 3.1: Test Setup

A high-speed camera was placed in front of the setup shown in Figure 3.1b, facing the setup straight-on. A meter stick was also placed on a table in front of the test setup to be used as a measurement reference when reviewing the videos, which can be seen in Figure 3.2. The test setup remained the same throughout the testing procedure, with the voltage, current, and/or the movable electrode speed being altered.

3.2 Data Extraction

The raw test data in the form of videos and text files did not provide enough information to successfully develop an expression and model for an arc naturally extinguishing in air. Because much of the analysis regarding natural arc extinction in air concerned the arc distance, which was not provided in the raw testing data, it had to be extracted using image processing techniques. These distances were utilized in the normalization of the resistances and later in the development of the ATP-EMTP models' arc resistance calculations. Furthermore, extracting and filtering the test data allowed for plotting and visualization to observe and understand the behaviors apparent in the arcs in air, which helped in developing the expressions and models for natural arc extinction in air.

3.2.1 Video Data

As evidenced by the stills in Figure 3.2, simply extracting the arc distances from the meter stick in the videos was entirely unattainable. The videos' graininess, poor lighting, and unpredictability of the arc warranted a more systematic, robust approach to extract arc data from the videos to achieve the most accurate representations possible.

(a) Before the Arc

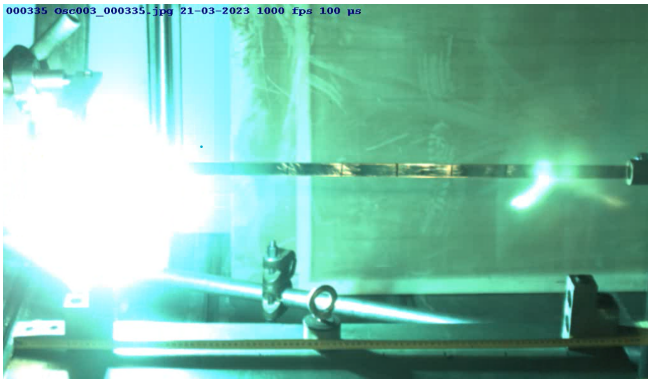

(b) During the Arc

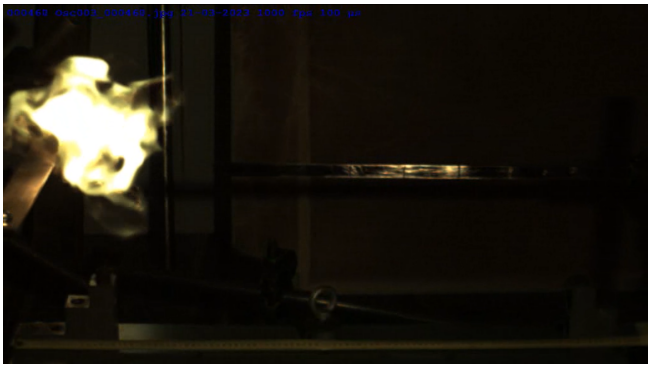

(c) After the Arc

Figure 3.2: Stills from an Arc Video: Before, During, and After the Arc

This process utilized the MATLAB image processing toolbox to isolate the arc image and extract its measurements (see Appendix A). First, the video file was loaded into MATLAB. A 1:1 scale between pixels and distance (in millimeters) was used across all videos. All videos had the same resolution. A matrix representing each video frame was created so that every individual frame could be manipulated as needed to extract the arc data. The arc image was isolated by adjusting the frame to grayscale to increase the image's sharpness. The image was then binarized so that the arc was a white figure against a black background, further isolating the arc image—which is demonstrated in Figure 3.3.

(a) Grayscale Arc Video Frame

(b) Binarized Arc Video Frame

Figure 3.3: Arc Image Isolation via MATLAB Image Processing

Bounding boxes were then created around every white object within the frame using the MATLAB image processing toolbox. Properties of each bounding box encompassing an object (such as the box width, height, location, etc.) were extracted. The box width was of particular interest because it correlated with the approximate arc distance. A filter was established to omit the bounding boxes that were too small to surround the arc and those too far from the arc location in the frame (because the arc occurred in the same area in each frame of every video), the results of which are displayed in Figure 3.4. The remaining bounding boxes were sorted by width to determine which box contained the actual arc image; the arc image was almost always contained within the widest bounding box. Once the correct bounding box had been found, its width (corresponding to the arc distance) was extracted and recorded.

Figure 3.4: Green Bounding Box Surrounding Arc Image

This arc distance was then plotted for each frame to visualize the relationship of arc distance with respect to time, as shown in Figure 3.5. It is worth noting that the time references of these plots were according to the frame rate of the high-speed videos and not the real-time duration of the arc; the arc distances were normalized to the correct real-time duration (along with the arc resistances) later on in the data processing. Finally, the arc distance data for each frame of the video were exported to an Excel spreadsheet for further analysis and manipulation. This process of finding the distance in every video frame was repeated for all 21 tests.

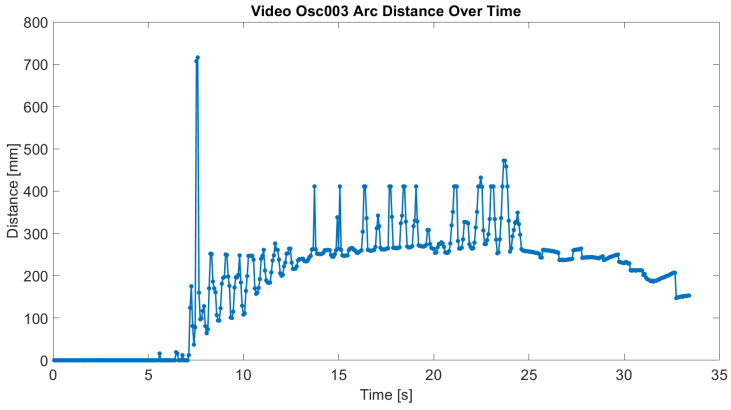

(a) Arc Distance, Video 3

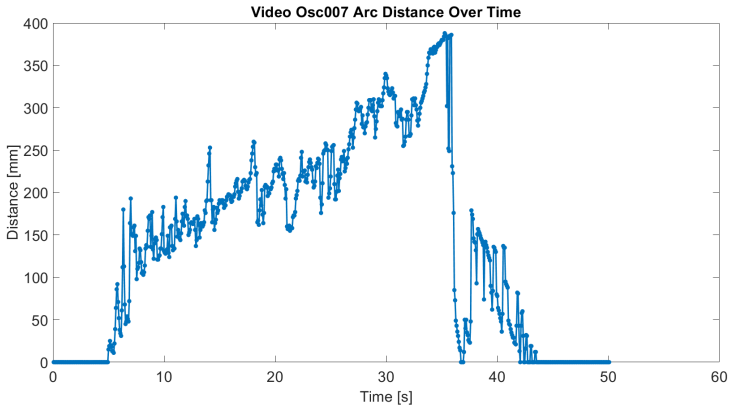

(b) Arc Distance, Video 7

Figure 3.5: Arc Distance Plot Examples

As evidenced by the distance fluctuations in Figure 3.5a and Figure 3.5b, the image processing tools used did not account for the light emanating from the arc and its flickering, affecting the perceived arc distance and potentially causing the extracted arc distance to be greater than its "true" arc distance. However, the quality of the videos did not allow for any more accurate measurements to know the "true" arc distance, arc reach, or arc length. To compensate for this potential shortcoming in data collection, a linear approximation was applied to the most linear, core segment of the arc's distance over time. This linear approximation was then extrapolated across the duration of the arc to obtain more accurate, linear arc distance data. The forthcoming arc calculations, derivations, and modeling in this thesis utilized these approximated arc distances, which were found for all 21 arc videos.

3.2.2 Oscilloscope Data

Unfiltered current and voltage oscilloscope data were provided along with the corresponding videos. These data were loaded into MATLAB for plotting and filtering. The voltage plots were highly noisy, so a fourth-order low-pass Butterworth filter was applied to accurately depict the voltage signal. A low-pass Butterworth filter was chosen because it provided a smooth response that removed any higher frequency noise apparent in the oscilloscope data, as opposed to a Chebyshev filter that has greater ripple due to its steeper roll-off [20]. A fourth-order filter was ultimately chosen because it provided a slightly steeper roll-off than a lower-order Butterworth filter but less steep than that of a Chebyshev filter. Roll-off refers to the filter's pass-band slope [20]. Although the current data were clean when plotted, the voltage filter shifted the data, so the current data were also filtered to account for that shift. The resulting voltage and current signals of one test (Test 3) are shown in Figure 3.6. The resistance values were calculated from these values using the basic Ohm's law equation (Equation 2.1). This process was also repeated for all 21 testing scenarios.

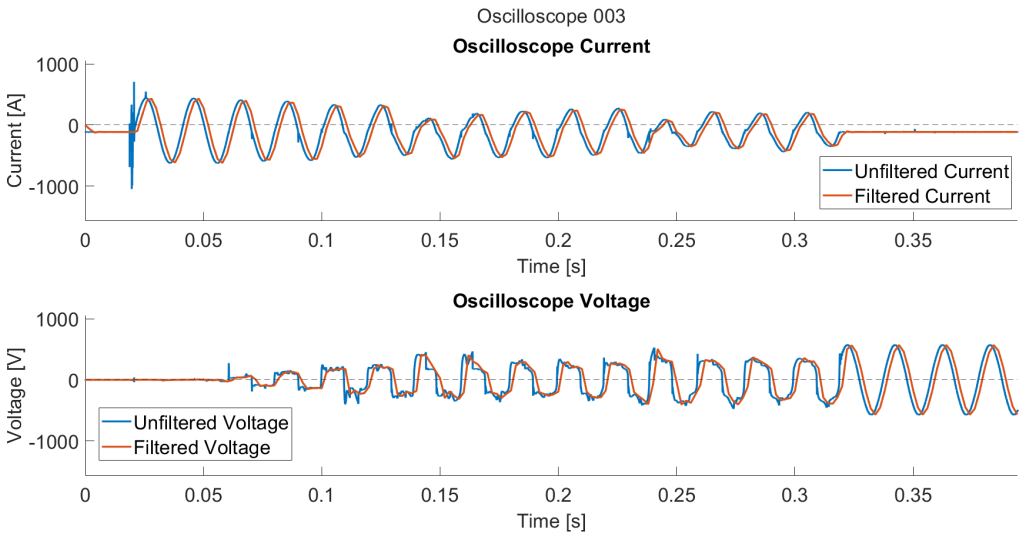

Figure 3.6: Oscilloscope Current and Voltage Data, Video 3

3.2.3 Normalizing Video and Oscilloscope Data

The frame rate, time steps, and arc distances across the videos and oscilloscope data were not uniform; comparison and data manipulation across these non-uniform data would have led to inaccurate results. Therefore, the test data received and extracted were normalized to mitigate this problem.

Normalizing Frame Rate/Video Time Steps

The video data employed different time intervals for different frame rates and speeds; the time steps provided in the videos did not correspond to the real-time duration of the arc. To obtain the real-time steps of the arc, the frame number corresponding to a specific moment in time was divided by the frame rate in frames per second (fps). The approximated arc distance discussed in subsection 3.2.1 used this normalized, real-time step.

Normalizing Oscilloscope Data to Video Distances

The voltage and current datasets from the oscilloscopes were significantly larger than those of the videos because of their differing frame rates. The voltage and current data were resized to match the time steps of the corresponding video (using the 1000 fps or 500 fps frame rates), so the arc voltage, current, resistance, and distance data from the oscilloscopes and video had the same vector lengths (see Appendix B for the source code).

Normalizing Resistances

Because arc resistance is strongly influenced by the arc distance, the arc resistances across the different arcing scenarios are not compatible for comparison. The resistances were normalized by their distance to produce normalized resistances that could be compared across the different arcing scenarios and used for developing an empirical expression describing natural arc extinction in air.

3.3 Data Filtering for Inverse Relationships

There exists an inverse relationship between a free-burning arc current and resistance; as the current decreases, the resistance increases. For each test, sequences of normalized resistance values and their corresponding currents were plotted to analyze the inverse resistance-current relationship. Observing the data on a small-scale level allowed for more detailed data processing and manipulation. The extracted, filtered data were then used to develop the mathematical expressions that describe the behavior of a naturally extinguishing arc in air from PED removal. This data filtering process to extract mathematical expressions describing the behavior of naturally extinguishing arcs in air is outlined in the following steps:

Step 1: Figure 3.7 illustrates an overview of the relationship between voltage and current with respect to time; from Ohm's law (Equation 2.1), voltage and current are proportional to one another. The voltage, current, and resistance relationships were inspected on a smaller scale, every half-cycle, to better analyze every individual point that comprised the resistance-current relationship of

that specific test. The black lines demarcate the exemplary half-cycle analyzed in the following steps.

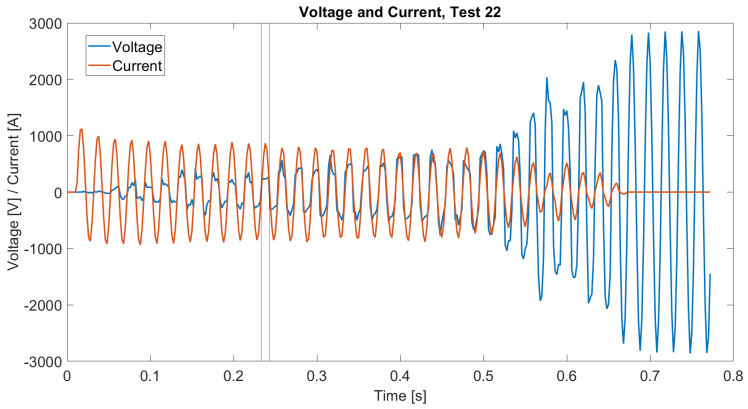

Figure 3.7: Voltage and Current, Test 22

Step 2: For example, Figure 3.8 showcases the extracted voltage and current half-cycle between 0.234 and 0.242 seconds. The arc resistance values were calculated from this voltage and current data.

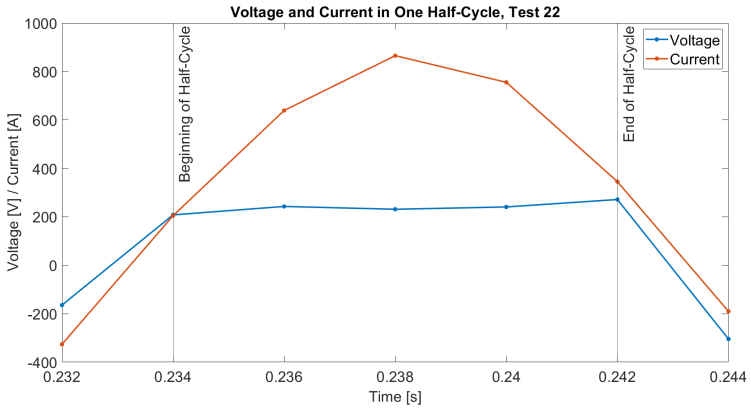

Figure 3.8: Voltage and Current in One Half-Cycle, Test 22

Step 3: The calculated arc resistances were normalized by the arc distances found in subsection 3.2.1, as discussed in section 3.2.3. The resulting normalized resistance values for the half-cycle are exhibited in Figure 3.9 with respect to time. The remainder of the steps employed these normalized resistances. Furthermore, the inverse resistance-current relationship becomes more apparent when comparing the normalized resistance values in Figure 3.9 and current in Figure 3.8.

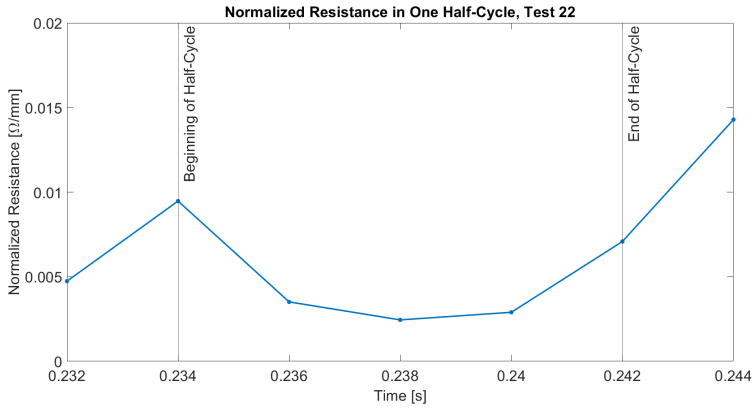

Figure 3.9: Normalized Resistance in One Half-Cycle, Test 22

Step 4: The normalized resistance values were then plotted against the current to determine if any sequence of points within the half-cycle exhibited the expected inverse resistance-current relationship. These sequences of points had to contain at least three successive points; omitting points within a sequence does not accurately reflect the arc's actual resistance-current relationship. Additionally, a minimum of three successive points were necessary to determine whether the inverse resistance-current relationship was present in the sequence. Due to the continuous nature of the arc and the imperfect nature of the test data, not all half-cycles exhibited this relationship and were therefore omitted from further analysis and comparison.

As in Figure 3.10, if multiple successive points in the half-cycle satisfied the relationship but not all as a single sequence, the sequence of values within that half-cycle that best satisfied the resistance-current relationship was chosen.

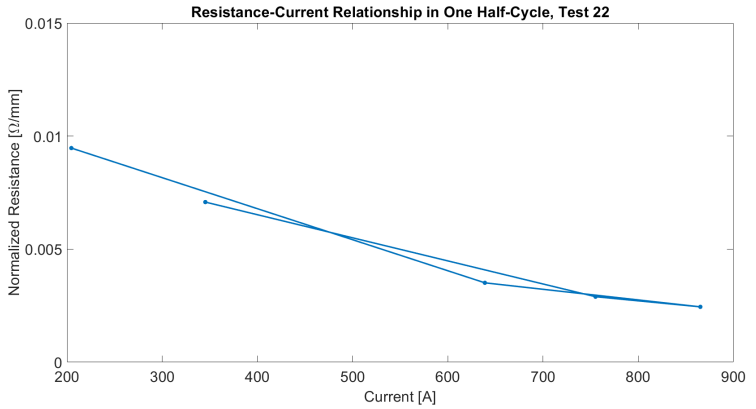

Figure 3.10: Resistance-Current Relationship in One Half-Cycle, Test 22

Within this particular half-cycle, there were two possible sequences of successive points that exhibited the expected inverse resistance-current relationship, sharing one common value, as Figure 3.11 demonstrates. The values corresponding to the yellow points were taken because they better exhibited the relationship of interest compared to the blue points, which is evidenced by the two corresponding sequences of data in Table 3.2 and Figure 3.11 (where the

green represents the shared value of the two possible sequences).

Current [A]	Normalized Resistance [Ω/mm]
204.612	0.0095
638.890	0.0035
865.203	0.0025
755.105	0.0029
345.294	0.0071

Table 3.2: Successive Points with One Shared Point in One Half-Cycle, Test 22

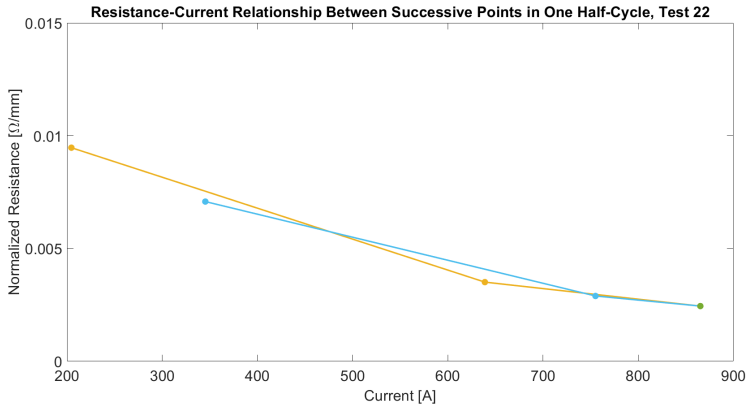

Figure 3.11: Successive Points with One Shared Point in One Half-Cycle, Test 22

Step 5: Steps 2 through 4 were repeated for every individual half-cycle within the arc test. The resulting filtered, normalized resistances corresponding to positive and negative currents were plotted separately to better observe the inverse resistance-current relationship and for fitting trendlines to the data. Some forms of expressions cannot contain both negative and positive values due to their asymptotic nature about the y-axis—so the positive and negative current values were split into two separate plots, and the absolute value of the negative current was taken. Any clear outliers, such as those Figure 3.12 displays, and their corresponding sequence of points (typically two other points) in that half-cycle were removed. The entire sequence corresponding to that point was removed to prevent disjointed sequences from influencing the data. Two trendlines were then fit to each data plot for comparison and analysis, one power law expression and one logarithmic expression of the form:

$$R = \kappa \cdot I^{\alpha} \quad [\Omega/mm] \tag{3.1}$$

$$R = \kappa \cdot log_{10}(I) + b \quad [\Omega/mm] \tag{3.2}$$

Where κ is a multiplication coefficient, b is the y-intercept value, and α is the power coefficient. Logarithmic and power law trendlines were chosen because both produced an inverse characteristic comparable to the resistance-current relationship observed in the naturally extinguishing arcs in air that were plotted in this research.

Figure 3.12 showcases the resulting trendlines (with outliers removed) for positive and negative current in Test 22. In Figure 3.12a and Figure 3.12b, the resistance-current relationships display the same behavior for both positive currents and negative currents, with comparable power law and logarithmic expression trendlines.

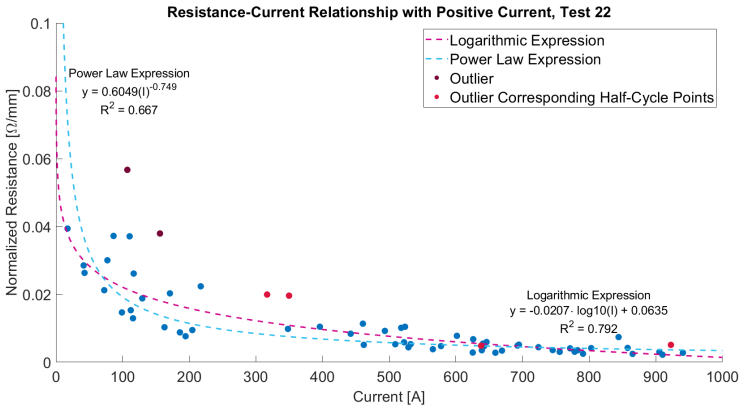

(a) Resistance-Current Relationship for the Positive Current, Test 22

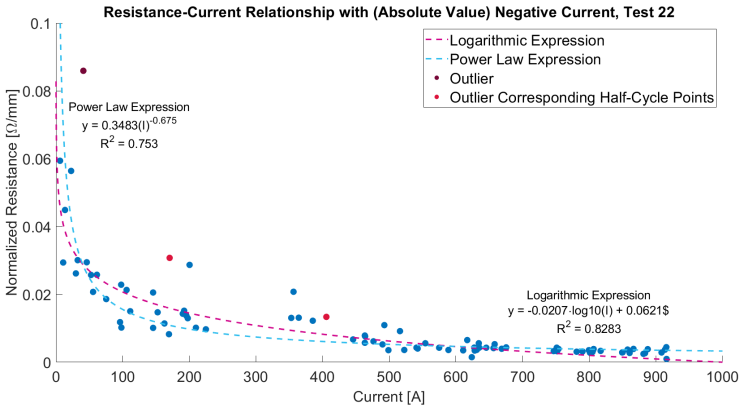

(b) Resistance-Current Relationship for the (Absolute Value) of the Negative Current, Test 22

Figure 3.12: Resistance-Current Relationships for Positive and (Absolute Value of) Negative Current, Test 22

This entire process was repeated for all 21 arc tests. The logarithmic and power law expressions for positive and negative current from each test are presented in Table 3.3. The resulting trendlines for positive or negative current that contained too few (fewer than 12) data points were omitted from the table. The trendlines are found in Table 3.3, where the gray rows denote the trendline values for the (absolute value of) negative current in each of the respective tests and the white rows the positive current in each respective test. The coefficient of determination values, R^2, of each expression were used to compare the accuracy of the power law expressions versus the logarithmic expressions. The coefficient of determination measures the goodness of fit of each calculated expression.

	Logarithmic			Power Law		
	κ	b	R^2	κ	α	R^2
Test 1	-0.0007	0.0015	0.7675	0.0077	-0.7600	0.6715
Test 3	-0.0161	0.0430	0.7933	0.5936	-0.9260	0.8102
Test 3	-0.0092	0.0247	0.7552	0.2569	-0.7680	0.7839
Test 4	-0.0368	0.0992	0.7042	1.6643	-0.9860	0.7124
Test 4	-0.0161	0.0495	0.7778	0.7960	-0.8540	0.8349
Test 5	-0.0507	0.1428	0.7442	2.4747	-0.9560	0.9711
Test 5	-0.0276	0.0839	0.7530	0.5630	-0.7320	0.8003
Test 6	-0.0253	0.0734	0.7131	2.2438	-1.0310	0.8579
Test 6	-0.0138	0.0426	0.7263	0.3939	-0.7630	0.8692
Test 7	-0.0184	0.0590	0.6814	2.4240	-1.0040	0.7664
Test 7	-0.0207	0.0647	0.6184	0.9486	-0.8410	0.7868
Test 8	-0.0207	0.0615	0.6868	2.4237	-1.0260	0.8180
Test 8	-0.0138	0.0450	0.4730	0.8995	-0.8920	0.7716
Test 11	-0.0737	0.1909	0.5518	2.3983	-0.9520	0.5884
Test 12	-0.1681	0.4500	0.6717	6.4571	-1.0950	0.7667
Test 13	-0.0507	0.1338	0.8470	2.3738	-0.9870	0.8833
Test 14	-0.0391	0.1182	0.8740	11.0210	-1.1890	0.8565
Test 14	-0.0138	0.0462	0.7922	1.2200	-0.8860	0.8055
Test 15	-0.0276	0.0870	0.5762	3.3580	-1.0670	0.6854
Test 15	-0.0092	0.0321	0.5271	0.5044	-0.7950	0.6662
Test 17	-0.0645	0.1622	0.6715	1.7417	-0.9620	0.8889
Test 20	-0.0391	0.1115	0.8914	2.9595	-1.0510	0.8671
Test 22	-0.0207	0.0635	0.7915	0.6049	-0.7490	0.6660
Test 22	-0.0207	0.0621	0.8283	0.3483	-0.6750	0.7525
Test 23	-0.0161	0.0481	0.9297	0.6331	-0.8120	0.7326
Test 23	-0.0161	0.0494	0.8060	0.8958	-0.8740	0.8785
Test 24	-0.0115	0.0349	0.8199	0.3159	-0.7040	0.7908
Test 24	-0.0138	0.0419	0.8010	0.3549	-0.7200	0.6064
Test 26	-0.0184	0.0553	0.8739	0.6193	-0.7890	0.7554
Test 26	-0.0184	0.0574	0.7839	0.1490	-0.5770	0.5476

Table 3.3: Calculated Logarithmic and Power Law Trendline Values for Test Data

After expressions were generated for all positive and negative resistance-current sequences across the testing scenarios with enough data to develop a trendline, mean representative expressions for all the power law and logarithmic expressions were calculated. These averaged expressions are meant to best encapsulate the typical

arc resistance-current relationship found across the test data available and form the basis of expression and model comparison for the remainder of this thesis.

To take these averages, the geometric mean was chosen over the arithmetic mean for accuracy; geometric means are often used to find the average of multiple or fluctuating rates, whereas the arithmetic mean is used when there is little variation or fluctuation in the data. The formula for the geometric mean is the following [21]:

$$\left(\prod_{i=1}^{n} x_i\right)^{\frac{1}{n}} = \sqrt[n]{x_1 x_2 \cdots x_n} \tag{3.3}$$

The comparative values of these two types of calculated means are found in Table 3.4.

	Logarithmic			**Power Law**		
	κ	b	R^2	κ	α	R^2
Arithmetic Mean	-0.0279	0.0763	0.6947	1.6139	-0.8257	0.7248
Geometric Mean	-0.0209	0.0614	0.7323	0.9057	-0.8692	0.7667

Table 3.4: Calculated Arithmetic and Geometric Mean Values

The geometric mean cannot consider negative values, so the absolute value of any negative values was taken. The negative sign was then reintroduced to the calculated constant value. The resulting power law and logarithmic expressions, utilizing the forms in Equation 3.2 and Equation 3.1, are then:

$$R = 0.9057 \cdot I^{-0.8692} \quad [\Omega/mm] \tag{3.4}$$

$$R = -0.0209 \cdot log_{10}(I) + 0.0614 \quad [\Omega/mm] \tag{3.5}$$

From the coefficients of determination in Table 3.4, the overall accuracy of the power law and logarithmic expressions was within approximately 4% of each other, justifying further comparison between the two expressions to determine which is better.

To further compare the two mathematical expressions, the power law and logarithmic expressions (Equation 3.4 and Equation 3.5, respectively) were plotted alongside one another in Figure 3.13. Both expressions exhibit similar behavior—decreasing nonlinearly with increasing current—as expected due to the inverse resistance-current relationship that the expressions are modeling. The power law expression spanned a greater (and higher) range of normalized resistance values compared to the logarithmic expression. The normalized resistance and current ranges for the logarithmic expression appeared to be more rigid than the power law expression, having distinct x- and y-axis intercept points, whereas the power law expression tended toward infinity in both the x- and y-directions, where the x-axis is representative of the normalized resistance values and the y-axis is representative of the current. These normalized resistance and current ranges could influence the rate—and ability—of

the arc model's extinction at current equal to 0 A.

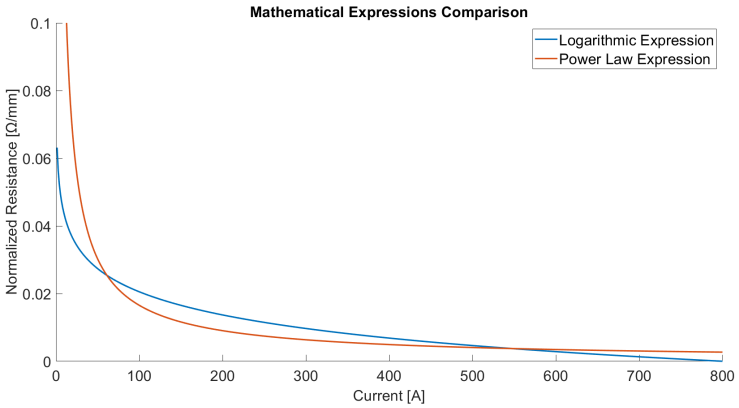

Figure 3.13: Mathematical Expression Comparison

3.4 Model Development

Modeling the mathematical expressions previously derived in this thesis allows for greater examination into how the expressions work and hold up to simulated testing conditions. These models also introduce any potential shortcomings of the derived expressions to allow for more detailed adjustments of the parameters to obtain the most accurate model and mathematical expressions possible.

The model was built based on the literature discussed in chapter 2 and the mathematical expressions found in section 3.3. Two separate models, one for the power law expression and one for the logarithmic expression, were developed for comparison. The power law and logarithmic arc models were based on the testing conditions and data of Test 23 (from Table 3.1), with an applied voltage of 2 kV_{rms}. The circuit resistance and inductance values were found using the following formulae:

$$Z = \frac{V_{rms}}{I_{rms}} \quad [\Omega] \tag{3.6}$$

$$R = Z \cdot cos\phi \quad [\Omega] \tag{3.7}$$

$$X = Z \cdot sin\phi \quad [\Omega] \tag{3.8}$$

$$L = \frac{X}{2\pi f} \quad [H] \tag{3.9}$$

$$\phi = arctan(\frac{X}{R}) \tag{3.10}$$

Where V_{rms} is the applied voltage and I_{rms} is the corresponding current. The $\frac{X}{R}$ ratio was taken to be 40 because the arc source was initially assumed to be a transformer, and $\frac{X}{R} = 40$ is typical for a transformer-fed source.

In addition to these basic components, a MODELS-language module containing the code that calculated the arc resistance was connected to a variable resistor, which represented the arc. As the distance, and thus variable arc resistance, increased with

time, the arc current decreased proportionally until the current reached 0 A.

3.4.1 Building the Reference Model

The reference model's purpose is to provide insight into the expected behaviors of the arc voltage, current, and resistance in the ATP-EMTP model simulation environment. [2] formed the basis of this reference model with its provided MODELS code and similar testing conditions. The resulting ATP-EMTP model can be seen in Figure 3.14, based on the schematics referenced in Figure 2.8. For this model and the following models, a 0.2 nF shunt capacitor was added. The shunt capacitor across the nonlinear arc resistor had little effect on the results, and its primary use was to filter a small amount of noise in the current waveform that would have been present otherwise.

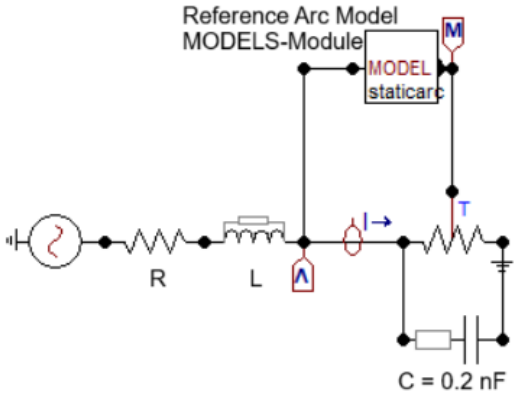

Figure 3.14: Reference Model Schematic

3.4.2 Building the Power Law Model

The power law expression parameters calculated in section 3.3 were utilized as the initial parameters for the arc resistance calculations in the MODELS module. However, these parameters caused the voltage waveshape to become concave down instead of the concave up shape expected [4][18]. The resistance expression parameters were then adjusted using curve fitting techniques to obtain the expected voltage waveshape and values. The final MODELS code for the power law expression-based model can be found in Appendix C, and the model schematic can be seen in Figure 3.15, where the arc initiation time, topen, was chosen arbitrarily (in this research and for comparison, to equal that of the Test 23 arc initiation time). The circuit schematic remained the same as in Figure 3.14, with the key difference being the different arc model MODELS-language module. These MODELS-language modules are the primary drivers of this thesis's arc model simulations.

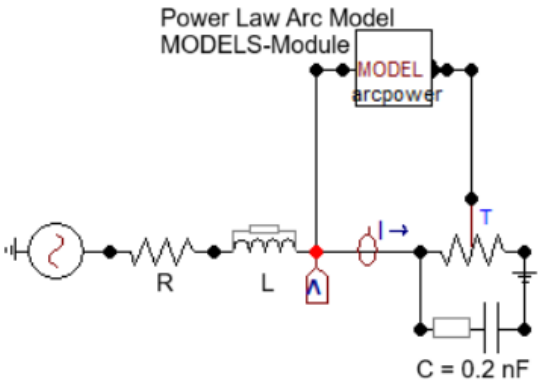

Figure 3.15: Power Law Model Schematic

3.4.3 Building the Logarithmic Model

As in the power law expression-based model, the logarithmic arc resistance expression constituted the initial parameters for the MODELS module arc resistance calculations. The final MODELS code for the logarithmic expression-based model is found in Appendix D, and the model schematic with the logarithmic arc model MODELS-language module is provided in Figure 3.16. The arc initiation time was chosen to be the same as with the power law expression model.

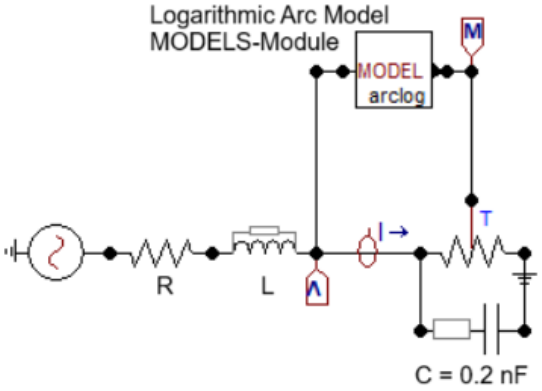

Figure 3.16: Logarithmic Model Schematic

3.4.4 Comparisons with Test Data

A MATLAB algorithm (see Appendix E) comparing the test data from Test 23 with the model simulation helped determine the accuracy of the model and its parameters. The results of these comparisons are discussed in chapter 4.

3.5 Plotting Natural Arc Extinction Distances

The arc model was applied to various testing conditions to compare the natural arc extinction distances simulated via this research's arc model with those found in [1]. The voltages were chosen to be within the range 200 V to 2400 V; the current was chosen to be within the range 200 A to 1000 A. Arc distances were found for three equivalent source impedances (voltage/current ratios): $U/I = 1\,\Omega$, $U/I = 2\,\Omega$,

and $U/I = 3\,\Omega$; and the power factor, $cos\phi$, was chosen to be 0.9 [1]. These changes were made within the ATP-EMTP circuit voltage source and series resistor and inductor; the MODELS-based arc resistance module and nonlinear resistor (the basis of the arc model) were not altered. The resistance and inductance values for each of the ratios are found in Table 3.5, using Equation 3.7, Equation 3.9, and

$$X = \sqrt{Z^2 - R^2} \quad [\Omega]$$

U/I [Ω]	**R** [Ω]	**X** [Ω]	**L** [mH]
3	2.70	1.31	4.16
2	1.80	0.87	2.77
1	0.90	0.44	1.39

Table 3.5: Electrical Parameters

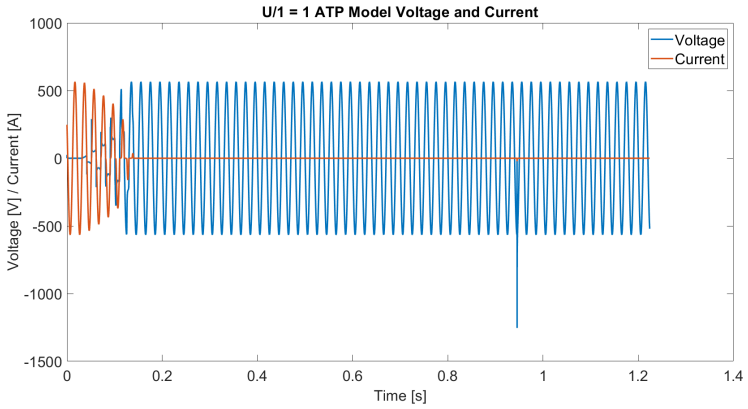

(a) U/I = 3 ATP Model Voltage and Current, 400 V_{rms} / 400 A_{rms}

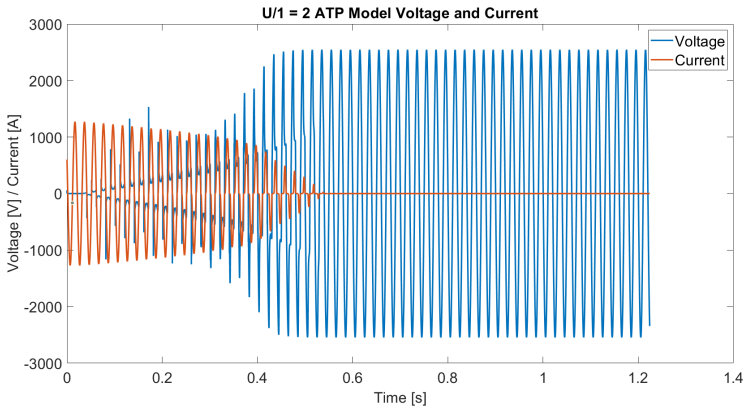

(b) U/I = 3 ATP Model Voltage and Current, 1800 V_{rms} / 900 A_{rms}

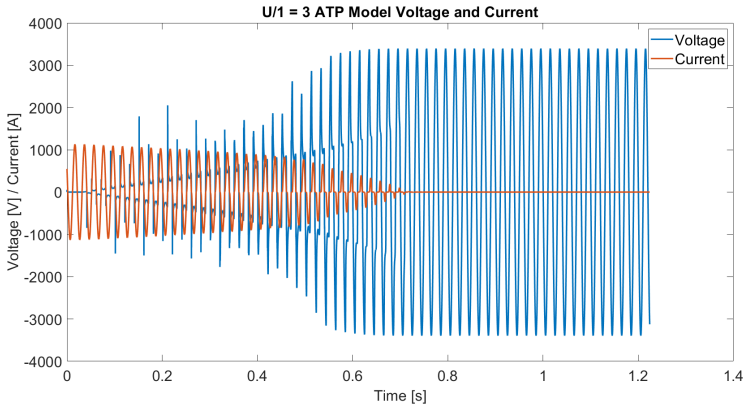

(c) U/I = 3 ATP Model Voltage and Current, 2400 V_{rms} / 800 A_{rms}

Figure 3.17: U/I Source Impedance Examples

For each of the three voltage/current ratios, the developed arc model utilized a series of voltages (and corresponding currents) as different test conditions for finding the arc extinguishing distances, as presented in Table 3.6. Figure 3.17 presents three such testing conditions for each of the source impedance (U/I) ratios. As seen in Figure 3.18, these distances were then plotted against their corresponding $\sqrt{U \cdot I}$ values, which represent the hypothesized arc distance relationship discussed in [1]. These values were compared to determine whether this empirical relationship held for the arc model found in this thesis.

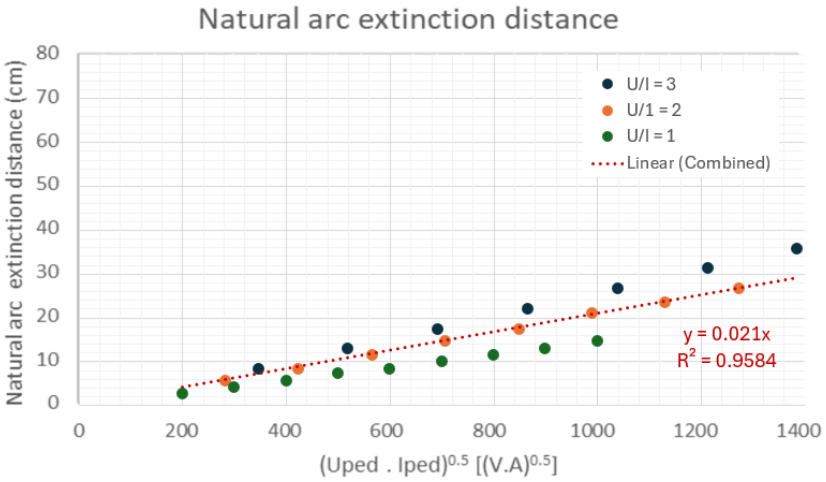

Figure 3.18: Arc Distance from Power Law Arc Model

Voltage [V_{rms}]	Current [A_{rms}]	$\sqrt{U \cdot I}$ [$\sqrt{VA}$]	Distance [cm]	Time [s]
1000	1000	1000	14.60	0.3103
900	900	900	13.03	0.2803
800	800	800	11.46	0.2503
700	700	700	9.88	0.2203
600	600	600	8.30	0.1903
500	500	500	7.26	0.1703
400	400	400	5.68	0.1403
300	300	300	4.11	0.1103
200	200	200	2.53	0.0803

(a) 1 Ω Testing Conditions

Voltage [V_{rms}]	Current [A_{rms}]	$\sqrt{U \cdot I}$ [$\sqrt{VA}$]	Distance [cm]	Time [s]
1800	900	1273	26.68	0.5403
1600	800	1131	23.53	0.4803
1400	700	990	20.90	0.4303
1200	600	849	17.23	0.3603
1000	500	707	14.60	0.3103
800	400	566	11.46	0.2503
600	300	424	8.31	0.1903
400	200	283	5.68	0.1403

(b) 2 Ω Testing Conditions

Voltage [V_{rms}]	Current [A_{rms}]	$\sqrt{U \cdot I}$ [$\sqrt{VA}$]	Distance [cm]	Time [s]
2400	800	1386	35.60	0.7103
2100	700	1212	31.40	0.6303
1800	600	1039	26.67	0.5403
1500	500	866	21.95	0.4503
1200	400	693	17.23	0.3603
900	300	520	13.03	0.2803
600	200	346	8.31	0.1903

(c) 3 Ω Testing Conditions

Table 3.6: Natural Arc Extinction Distance Testing Conditions

3.6 Conclusions

This methodology chapter aims to describe the various processes and techniques employed to reach the final mathematical expressions and models that will be discussed in the following chapter. The test setup under which the test data were received and used for the duration of this research is described to clearly illustrate the testing conditions and potential for this thesis's work. To first obtain usable data from these given test files, the arc distances had to be extracted from the arc videos using image processing techniques. The raw oscilloscope data were filtered, and the resistances were calculated from those values. The distance time steps, voltage and current oscilloscope data, and resulting resistances were all normalized for the comparison and development of averaged mathematical expressions that describe the arcs' resistance-current relationship. These averaged expressions were then employed in two potential arc model simulations using ATP-EMTP software, which

will be compared and contrasted with each other and the reference test data in the following chapter. Finally, the arc model was employed to find the natural arc extinction distances under different testing conditions for comparison with the findings in [1], from which this thesis's problem is formulated.

Chapter 4

Results and Discussion

This chapter presents the research findings of this thesis, discussing their significance in the context of natural arc extinction in air from PED removal. The results focus on the mathematical expressions and their respective ATP-EMTP model simulations. These expressions and calculations aim to find the arc resistance in terms of current and arc distance. The normalized arc resistance expressions were multiplied by the arc distance with respect to time to obtain the actual arc resistance, which grew over time until the arc successfully extinguished. Furthermore, due to the iterative nature of the variable arc resistance calculations over time, the solution can get stuck between two points in a given iteration, which then acts as an amplifier. However, this behavior does tend to replicate the chaotic and random nature of a free-burning arc in air. This chapter investigates the calculated arc resistances over time and the resulting U-I characteristics of the arc, comparing them with the test data from [7] to determine each model's accuracy and explain their impact in understanding how a free-burning arc in air extinguishes.

4.1 Power Law Model Results

The power law arc expression and its corresponding ATP-EMTP model demonstrate a free-burning arc in air's behaviors and its ability to self-extinguish. The parameters of the power law expression were adjusted according to curve fitting techniques to better fit the testing conditions. The expression for the arc resistance, considering only the current and arc distance, then becomes:

$$R_{arc} = (6.21308 \cdot I^{-1.041308} - 0.002) \cdot d \quad [\Omega] \tag{4.1}$$

Where d is the arc distance at an instant in time. The current range for this expression was tested up to approximately 1000 kA_{rms} with a maximum distance of one meter, per the testing conditions in [1][7]. Figure 4.1 illustrates these behaviors: while the arc occurs, the arc voltage and current are in phase with each other; the arc voltage increases with time as the arc current decreases; and once the arc self-extinguishes, the current remains at 0 A, and the voltage begins to oscillate at its pre-arc steady-state value. A free-burning arc in air is primarily resistive (with any inductance being negligible compared to the resistance), causing the voltage and current waveforms to be in phase [4]. It is also worth noting that the overvoltage spikes in the simulation figure result from how an inductor is simulated in ATP-EMTP software

in the model circuit; these overvoltages would not be present in a real-life arcing scenario.

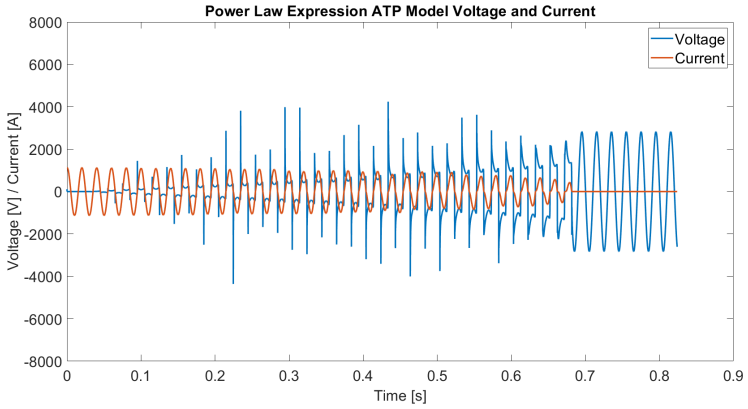

Figure 4.1: ATP-EMTP Calculated Arc Voltage and Current, Power Law Expression

4.1.1 Resistance

Understanding the arc resistance and its role in a free-burning arc in air precedes an understanding of the behaviors and characteristics present in naturally extinguishing arcs in air. The arc's extinguishing distance is proportional to its arc resistance. Figure 4.2 showcases the calculated arc resistance that the model simulations are based on. These results agree with those found in [2][11][15] and as discussed in chapter 2. However, unlike these more static models, the power law expression causes the resistance to increase more rapidly with time, which, in turn, causes the current to decrease until the arc extinguishes.

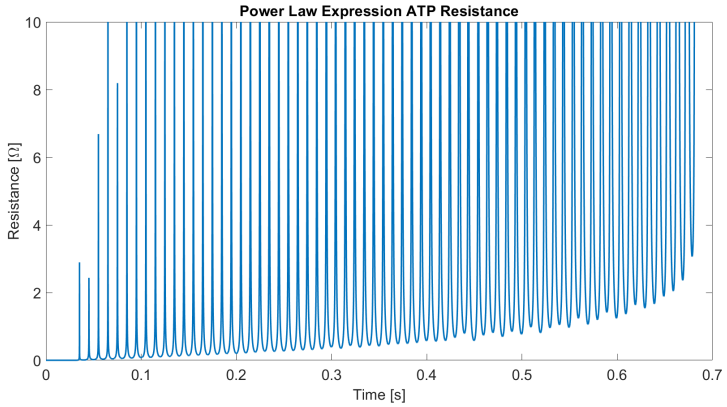

Figure 4.2: ATP-EMTP Calculated Arc Resistance, Power Law Expression

In the model, from Figure 3.15, the calculated arc resistance was fed into a nonlinear resistor (representing the arc) that then influenced the current and voltage. As evidenced in Figure 4.2, there is no resistance present in the nonlinear resistor before the arc initiates, and the resistance grows with increasing time and distance until it is large enough to drive the arc current to remain at 0 A, thus extinguishing the arc. The spikes in resistance occur at current zero-crossings, where the resistance briefly becomes arbitrarily large.

4.1.2 U-I Characteristic

A free-burning arc in air's resistance, voltage, and current are interdependent. The calculated arc resistance will shape the voltage and current's behavior and characteristics. The arc's U-I characteristic curve visualizes these characteristics and relationships. Figure 4.3 demonstrates a U-I characteristic with an inverse arc voltage and current relationship for both positive and negative currents. This inverse voltage-current relationship mirrors the resistance-current relationship described in chapter 3 and from which the power law expression is derived.

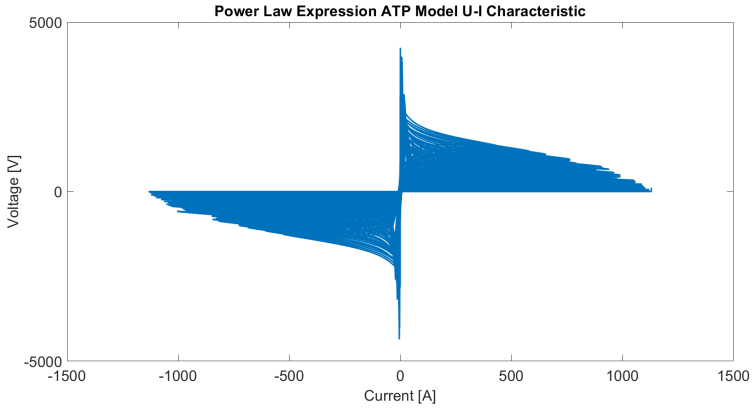

Figure 4.3: U-I Characteristic Curve, Power Law Expression

Furthermore, Figure 4.3 showcases a hysteresis loop-type shape, expressing that different voltages are possible—due to the varying arc distances—with the same current values [4]. The larger voltages correspond to longer arc distances and a shorter current range, reinforcing the claim that increasing arc distance is a main driver in the arc's natural extinction.

4.1.3 Comparison to Test Data

The accuracy of the power law expression is best exemplified by comparing the ATP-EMTP model results with the received test data. The test data from Test 23 (see Table 3.1) best correspond to the testing conditions applied in the ATP-EMTP model simulations, so the following comparisons are between these two datasets. While comparisons of the model simulations to relevant literature are beneficial in perceiving the arc's behaviors in the context of existing research, comparing the model results with the test data that recreated the arcing conditions provides a clearer outlook on the model's applicability in real-world situations.

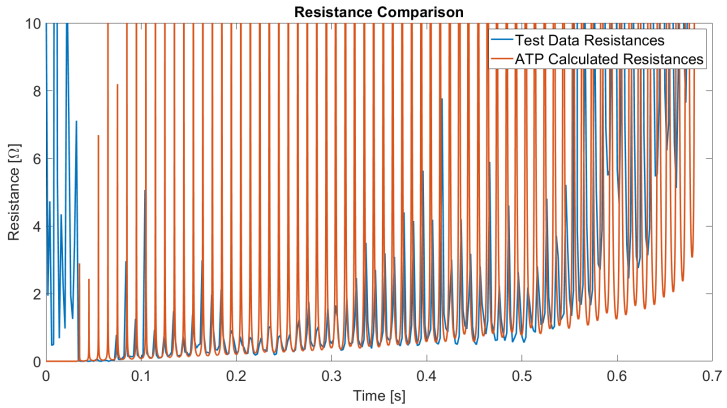

Figure 4.4: Comparison Between the Test Data Resistance and ATP-EMTP Calculated Resistance, Power Law Expression

The initial resistance before arc initiation that is present in the test data does not pertain to the actual arc resistance and is a result of using Ohm's law (Equation 2.1) to find the test data's resistance values; only the arc resistance after arc initiation were considered in this comparison. As shown in Figure 4.4, for most of the arc's duration—from initiation to approximately 0.55 s of simulation—the calculated arc resistance values closely replicate the arc resistance values. The primary difference is the calculated arc resistance at current zero-crossings going to a higher arbitrarily large resistance value, which makes little difference in the arc's behavior, due to when these spikes occur. After approximately 0.55 s into the simulation, the real arc resistance begins increasing at a faster rate and becomes slightly more erratic than the calculated arc resistance. This difference in resistance values after 0.55 s is potentially due to the longer arc distance in the tests from [7] compared to the distances between the electrodes found in the simulations.

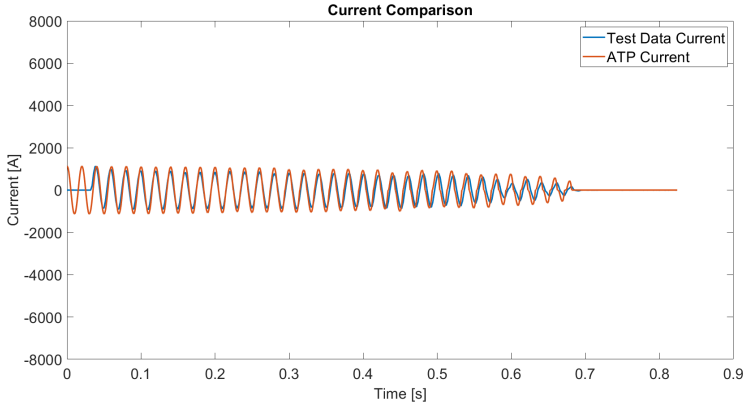

Figure 4.5: Comparison Between the Test Data Current and ATP-EMTP Calculated Current, Power Law Expression

Figure 4.5 displays a slight difference in amplitudes between the test data current and the ATP-EMTP model current, which is likely due to how the ATP-EMTP circuit's linear resistor and inductor were calculated. The calculated arc resistance (which has a slower growth rate as the arc nears extinction at the end of the simulation) could also be a cause for the current to decrease at a slower rate than the

test data current. However, both currents retain the same shape and extinguish at approximately the same time, which is the most significant aspect of this research.

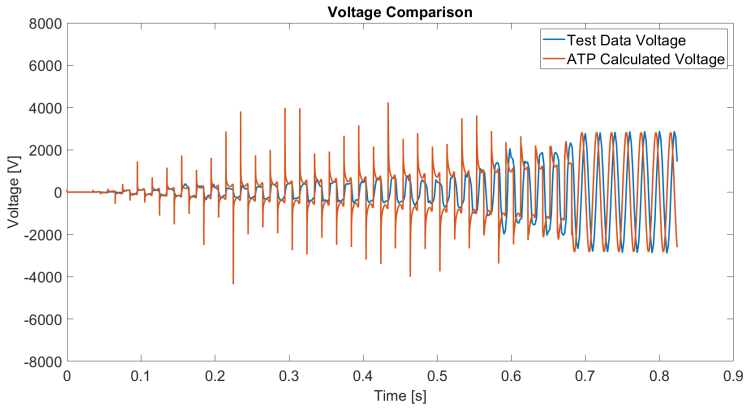

Figure 4.6: Comparison Between the Test Data Voltage and ATP-EMTP Calculated Voltage, Power Law Expression

In Figure 4.6, the calculated arc voltage closely follows the shape of the test data's arc voltage, with the main divergence occurring at the same instances where the calculated arc resistance diverges from the test data arc resistance, as discussed above. The calculated arc voltage also increases to match the test data arc voltage amplitude after the arc extinguishes. This arc voltage comparison further augments the power law expression's ability to accurately model a naturally extinguishing arc in air, reflecting its nonlinear, dynamic behaviors.

4.2 Logarithmic Model Results

The logarithmic expression model aims to serve as a comparison to the above power law expression model, exemplifying a free-burning arc in air's dynamic behaviors. The logarithmic expression ATP-EMTP model simulation exhibits much of the expected arc behaviors described in chapter 2. Similarly to the power law expression, the logarithmic expression's parameters were adjusted to better fit the testing conditions. The logarithmic expression for arc resistance, considering only the current and arc distance, is then:

$$R_{arc} = (-0.2073 \cdot log_{10}(I) + 0.066) \cdot d \quad [\Omega] \tag{4.2}$$

The current and distance range for this expression are expected to be similar to those discussed for the power law expression.

However, unlike the results of the power law expression simulation, the logarithmic expression simulation's arc does not self-extinguish, as evidenced in Figure 4.7. While the arc current does slowly decrease with increasing voltage (and thus resistance), it does not do so at a rate sufficient to extinguish the arc, significantly impacting the efficacy of the model for naturally extinguishing arcs in air.

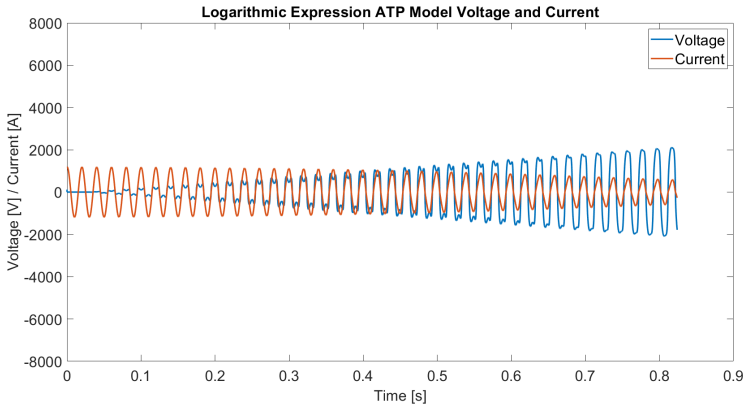

Figure 4.7: ATP-EMTP Calculated Arc Voltage and Current, Logarithmic Expression

4.2.1 Resistance

The calculated arc resistance is the primary mover of the arc model simulations, so its results further influence the arc voltage and current behavior. As shown in Figure 4.8, the calculated logarithmic expression model arc resistance produces similar results to the power law expression model and to the expected results found in chapter 2. However, this model's results begin to diverge as time progresses: the rate at which the resistance increases is much slower than that of both the power law expression model and the expected results.

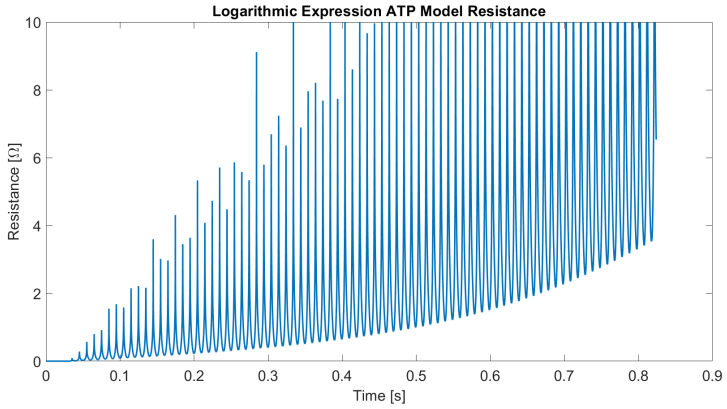

Figure 4.8: ATP-EMTP Calculated Arc Resistance, Logarithmic Expression

4.2.2 U-I Characteristic

The voltage-current relationship presented in the U-I characteristic establishes the arc resistance expression's influence on the arc's behavior. The U-I characteristic in Figure 4.9 exhibits a hysteresis loop-type shape, its voltage varies with the varying arc distance values, and the highest overall voltages have a smaller range of current values. However, the inverse voltage-current relationship is not present. This voltage-current relationship looks significantly different than that found in the power law expression model in Figure 4.3 and the U-I characteristics for free-burning arcs in air in chapter 2.

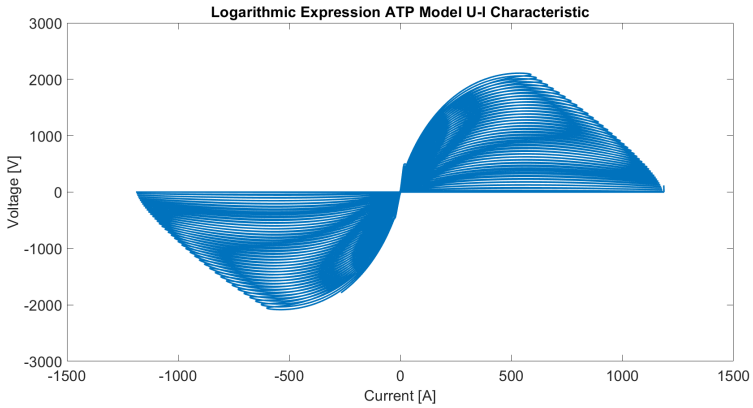

Figure 4.9: U-I Characteristic Curve, Logarithmic Expression

Comparing the simulated voltage-current characteristic of this logarithmic expression with those in [2][4][9][11][15] and the power law expression U-I characteristic above, its effectiveness in realistically describing a free-burning arc in air's behaviors is more dubious. The voltage-current relationship does not clearly reflect the resistance-current relationship from which the expression is derived.

4.2.3 Comparison to Test Data

To better understand the effects of these results in a more explicit context, the simulated model was plotted alongside the test data for Test 23. These comparisons help determine the plausibility of the logarithmic expression accurately simulating a free-burning arc in air's behaviors.

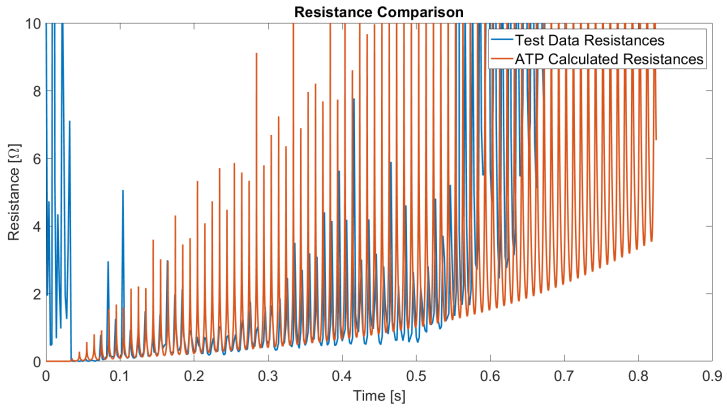

Figure 4.10: Comparison Between the Test Data Resistance and ATP-EMTP Calculated Resistance, Logarithmic Expression

As evidenced in Figure 4.10, the overall logarithmic arc resistance expression values vary significantly from the test data values. For the initial (approximately) 0.4 s, the calculated arc resistance is relatively consistent with the test data arc resistance. Nevertheless, after this point in time, the increasing rate of the calculated arc resistance expression is substantially slower, resulting in much lower resistance later in the arc's duration. This low resistance is not enough to cause the arc to extinguish during the simulation.

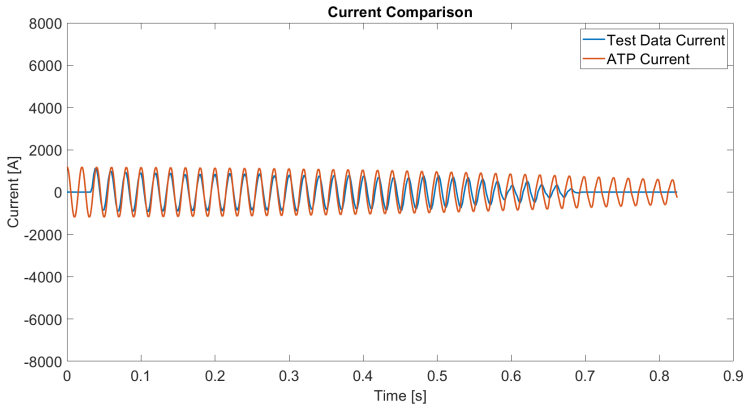

Figure 4.11: Comparison Between the Test Data Current and ATP-EMTP Calculated Current, Logarithmic Expression

The ATP-EMTP model's current amplitudes in Figure 4.11 are significantly greater than the test data current amplitudes—even more so than the difference evident in the power law expression model. Additionally, due to the low arc resistance values calculated, the rate at which the model current decreases is significantly slower than the test data current. The arc current is not brought to a sustained 0 A; the arc does not extinguish as expected in this model.

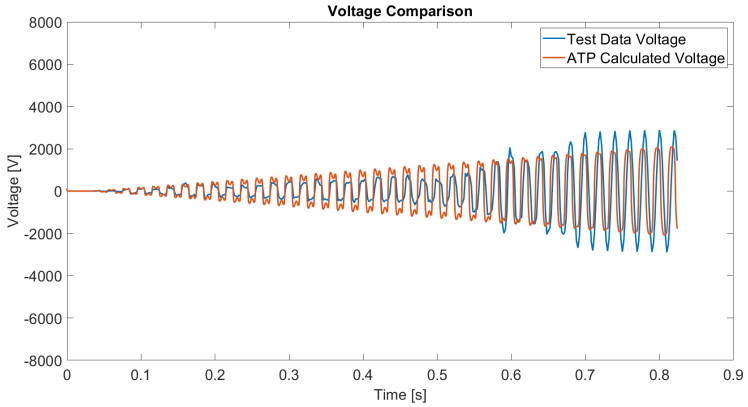

Figure 4.12: Comparison Between the Test Data Voltage and ATP-EMTP Calculated Voltage, Logarithmic Expression

The voltage comparison in Figure 4.12 demonstrates that the logarithmic expression model's voltage waveshape initially closely mirrors that of the test data. However, it quickly begins to deviate, becoming larger than the test data's waveshape for much of the arc's duration. The last moments before the test data's arc extinguishes, the logarithmic expression model's resulting arc voltage fails to increase at a rate sufficient to mimic the arc's extinction. The model does not extinguish, which is the primary concern of this research, therefore disqualifying the logarithmic model from being a suitable arc model for natural arc extinction in air during the removal of PEDs.

4.3 Natural Arc Extinction Distance Comparison

The natural arc extinction distance is paramount to describing naturally extinguishing arcs in air. The arc model's ability to reasonably predict this distance distinguishes it from previous research on static free-burning arcs in air. A dynamic arc model that sufficiently predicts the natural arc extinction distance provides deeper insights into the arc's behaviors. [1] hypothesized that the natural arc extinction distance is $5 \times 10^{-4} \cdot \sqrt{U \cdot I}$ cm. This hypothesis was tested by employing the power law model to predict the natural arc extinction distance under various testing conditions (outlined in section 3.5). The results of which were compared to those in [1].

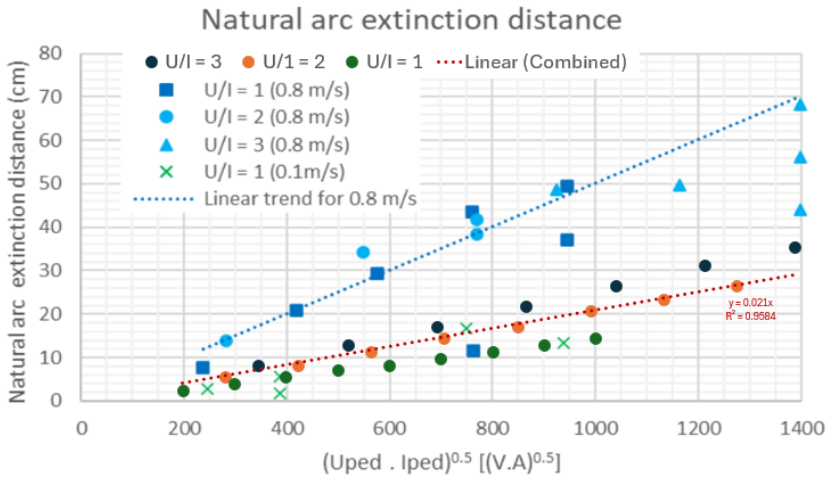

Figure 4.13: Natural Arc Extinction Distance Comparison with the Findings in [1]

As can be seen in Figure 4.13, both trendlines are almost perfectly linear. The trendline and datapoints derived from this model are expected to more closely match the 0.8 m/s data in [1] but instead match the 0.1 m/s results. However, due to the approximations that had to be made when extracting the arc distance from the videos (as detailed in subsection 3.2.1), the data in which this research model draws upon are imperfect. With more precise arc measurements and fine-tuning of the model parameters, the results should become more accurate. Despite the imperfect test data received, this research model does produce results with the same trend and within the same vicinity as the original findings in [1], further substantiating the claim that the natural arc extinction distance is proportional to $\sqrt{U \cdot I}$. This thesis's findings corroborate the hypothesis proposed with the original test data in [1]. In turn, the original test data's results substantiate the overall arc model's predictions, with the implication that the model may be improved by adjusting the model parameters.

4.4 Conclusions

Of the two mathematical expressions derived in this research, it is apparent that the power law expression and its corresponding model more accurately depict the dynamic behaviors of a naturally extinguishing arc in air. The power law expression and its model simulation closely mirror the real-life arc behaviors in their comparisons with literature and test data. Conversely, the logarithmic expression emerged

as significantly less accurate when compared to both the expected behaviors from literature and test data. Furthermore, its inability to demonstrate the self-extinguishing property of free-burning arcs in air eliminated it as a plausible candidate for describing natural arc extinction in air's behaviors. The power law expression model was then compared to the different conditions of the original test data, demonstrating the same trend with marginally different arc distance values. These differences may be mitigated by altering the model parameters in the presence of less ambiguous test data. This thesis's mathematical expressions and model simulations (and their resulting resistances, voltage-current characteristics, and arc extinction distances) were compared and analyzed against the backdrop of naturally extinguishing arcs in air resulting from PED removal. These results contextualize the research in understanding and characterizing naturally extinguishing arcs in air more accurately.

Chapter 5

Conclusion

5.1 Conclusions

The primary topic of this thesis is to better understand and model the behaviors of naturally extinguishing arcs in air when removing PEDs. Of the different arc-types reviewed from literature, free-burning arcs in air most closely resembled the naturally extinguishing arcs in air this thesis aimed to study due to their inductive and chaotic, dynamic behaviors. This thesis proposed that a naturally extinguishing arc in air that occurs when removing a PED can be described by the following mathematical expression:

$$R_{arc} = (6.21308 \cdot I^{-1.041308} - 0.002) \cdot d \quad [\Omega]$$

Whose arc model simulation successfully self-extinguished, exhibited the characteristics of free-burning arcs in air, and closely replicated the natural arc extinguishing distance hypothesized in [1]. In the arc model ATP-EMTP simulations employing a mathematical expression of the form:

$$R_{arc} = (\kappa \cdot I^{\alpha} + b) \cdot d \quad [\Omega]$$

Both the κ and α parameters influenced the resulting arc voltage and current's damping envelope shape, and thus arc extinction time and distance. Differing values of the κ parameter mirrored the chaotic, unpredictable nature of the arc, sometimes significantly shifting the arc extinction time and distance, and sometimes not. Both parameters must work in unison for the arc model to be successful. Furthermore, the arc model varied greatly with the representation of the source impedance (the circuit series resistance and inductance values); a more heavily resistive equivalent source impedance (or U/I ratio, as described in section 3.5) provided results that were more similar to the original test data findings in [1]. These values are highly sensitive and receptive, and a small change in the source impedance values can alter the entire arc characteristic in the model.

The objectives of this master's thesis are met, which are to establish a mathematical expression that describes a naturally extinguishing arc in air's behaviors and

to implement a working arc model based on the expression that verifies its accuracy through simulation. The mathematical expression formulated in this thesis and its corresponding arc model reasonably predict the arc voltage, current, resistance, and extinction distance (albeit with a scale factor difference of 2.4) despite utilizing largely approximated test data. As its predictions improve in the future, the arc model may augment testing—simplifying the processes of designing the arc tests and understanding their results—to study a naturally extinguishing arc in air's behaviors and arc extinction distance. The findings in this research also help to fill the gap of modeling dynamic free-burning arcs in air and predicting their extinction, which is present in the existing literature on arcs. Furthermore, this more easily accessible information and understanding of natural arc extinction in air can inform future safety protocols and procedures for the workers utilizing not only PEDs but also other grounding devices that could create arcs in de-energized circuits. Use of the arc model could potentially be extended to disconnector arcs during bus transfer, enhancing knowledge on its application and testing results.

5.2 Recommendations for Future Research

This thesis demonstrates the necessity for developing a mathematical expression and arc model that quantitatively depicts a naturally extinguishing arc in air's behaviors and characteristics. The research presented in this thesis forms the basis for that model, but it can be expanded upon to augment the model's performance and accuracy. In the expectation that future research will be carried out to build upon this research's findings, the following recommendations are proposed.

The first recommendation is for new testing that more clearly discloses the arc distance, arc reach, and arc length to improve the model's arc extinction distance predictions. This information will likely come in the form of arc videos (as it did in this research); videos in a higher resolution with better visibility of the arc could ameliorate this problem. However, it is worth noting that there is a tradeoff to consider between better visibility of the arc and visibility of the surrounding test setup during the arc.

The second recommendation is that arcs with different testing conditions and test setups than those performed at Damstra Laboratory should be investigated. This research utilized one set of test data from one laboratory. More testing will determine if the naturally extinguishing arc in air's characteristics are repeatable under different conditions in different settings and if this thesis's arc model remains accurate.

The final recommendation is that the ATP-EMTP model circuit should be further manipulated to clean the overvoltage spikes due to the circuit's inductor from the arc voltage signal. These overvoltage spikes are a product of how ATP-EMTP simulates inductors, and these effects are amplified during the software's iterations through the MODELS arc module across time. A cleaner voltage signal would provide a clearer impression of how the derived mathematical expression performs in the simulations.

Bibliography

[1] E. de Meulemeester, R. Bhuyan, S. Dhruvi, P. Kidambi, and C. Engelbrecht, "Considerations for Temporary Earthing in Compact and Heavy Loaded OHL," in *B2 PS1: Challenges from Renewables Integration and Influences of Energy Transition on OHL*, Paris: CIGRE, 2024.

[2] V. Terzija, G. Preston, M. Popov, and N. Terzija, "New Static "AirArc" EMTP Model of Long Arc in Free Air," *IEEE Transactions on Power Delivery*, vol. 26, no. 3, pp. 1344–1353, Jul. 2011, ISSN: 1937-4208. DOI: 10.1109/TPWRD.2010.2086082. [Online]. Available: https://ieeexplore.ieee.org/document/5743047 (visited on 02/28/2025).

[3] R. Smeets, L. van der Sluis, M. Kapetanovi, D. Peelo, and A. Janssen, *Switching in Electrical Transmission and Distribution Systems*. John Wiley & Sons Ltd, 2015, 424 pp., ISBN: 978-1-118-38135-9.

[4] Y. (Chai. "Capacitive current interruption with high voltage air-break disconnectors." (2012), [Online]. Available: https://research.tue.nl/en/publications/capacitive-current-interruption-with-high-voltage-airbreak-disconnectors(eb4d87bf-4ad6-41ee-8a93-e803c7a3f809).html (visited on 01/08/2025), pre-published.

[5] H. Ito, Ed., *Switching Equipment* (CIGRE Green Books). Cham: Springer International Publishing, 2019, ISBN: 978-3-319-72537-6 978-3-319-72538-3. DOI: 10.1007/978-3-319-72538-3. [Online]. Available: http://link.springer.com/10.1007/978-3-319-72538-3 (visited on 01/08/2025).

[6] L. van der Sluis, *Transients in Power Systems*. John Wiley & Sons Ltd, 2001, 207 pp.

[7] R. Wanschers, "Arc measurements for portable earth device (ped)," Prof. ir. Damstra Laboratory.

[8] H. H. Goh, S. Sim, N. Iskandar, and S. Mazlan, "Types of circuit breaker and its application in substation protection," *Indones J Electr Eng Comput Sci*, vol. 8, no. 1, pp. 213–220, 2017.

[9] D. F. Peelo, "Current Interruption Using High Voltage Air-Break Disconnectors," Technische Universiteit Eindhoven, Eindhoven, 2004, 168 pp.

[10] D. F. Peelo, *Current Interruption Transients Calculation*, 2nd ed. John Wiley & Sons Ltd, 2020, 282 pp.

[11] M. M. Saha, J. Izykowski, and E. Rosolowski, *Fault Locations on Power Networks*. Springer International Publishing, 2010, ISBN: 978-1-84882-885-8.

[12] E. Gross, "Free burning long power arcs at high voltage," *Schweizer Arkiv fűr Angewandte Wissenschaft und Technik*, vol. 19, 1941.

[13] K. Anjo, H. Terase, and Y. Kawaguchi, "Self-extinction of arcs created in long air gaps," *Electrical Engineering in Japan*, vol. 88, no. 4, 1968.

[14] A. S. Brilinskiy, G. A. Evdokunin, and A. D. Petrova, "Optimal free-burning AC arc model selection for electromagnetic transients in power systems," *IOP Conference Series: Materials Science and Engineering*, vol. 643, no. 1, p. 012 112,

Nov. 2019, ISSN: 1757-899X. DOI: 10.1088/1757-899X/643/1/012112. [Online]. Available: https://dx.doi.org/10.1088/1757-899X/643/1/012112 (visited on 02/28/2025).

[15] V. Terzija, G. Preston, M. Popov, and Z. Radojevic, "A New EMTP Model of the Long Arc in Free Air,"

[16] V. Terzija and H.-J. Koglin, "On the modeling of long arc in still air and arc resistance calculation," *IEEE Transactions on Power Delivery*, vol. 19, no. 3, pp. 1012–1017, Jul. 2004, ISSN: 1937-4208. DOI: 10.1109/TPWRD.2004.829912. [Online]. Available: https://ieeexplore.ieee.org/document/1308321 (visited on 03/14/2025).

[17] V. Terzija and H.-J. Koglin, "Long arc in free air: Testing, modelling and parameter estimation. I," in *Ninth International Conference on Harmonics and Quality of Power. Proceedings (Cat. No.00EX441)*, vol. 2, Oct. 2000, pp. 404–409. DOI: 10.1109/ICHQP.2000.897714. [Online]. Available: https://ieeexplore.ieee.org/document/897714 (visited on 03/28/2025).

[18] V. Terzija and H.-J. Koglin, "Long arc in free air: Testing, modelling and parameter estimation. II," in *Ninth International Conference on Harmonics and Quality of Power. Proceedings (Cat. No.00EX441)*, vol. 2, Orlando, FL, USA: IEEE, 2000, pp. 481–486, ISBN: 978-0-7803-6499-8. DOI: 10.1109/ICHQP.2000.897726. [Online]. Available: http://ieeexplore.ieee.org/document/897726/ (visited on 03/28/2025).

[19] V. Terzija and H.-J. Koglin, "Long arc in free air: Testing, modelling and parameter estimation. I," in *Ninth International Conference on Harmonics and Quality of Power. Proceedings (Cat. No.00EX441)*, vol. 2, Orlando, FL, USA: IEEE, 2000, pp. 404–409, ISBN: 978-0-7803-6499-8. DOI: 10.1109/ICHQP.2000.897714. [Online]. Available: http://ieeexplore.ieee.org/document/897714/ (visited on 03/28/2025).

[20] C. E. Free and C. S. Aitchison, *RF and Microwave Circuit Design: Theory and Applications* (Microwave and Wireless Technologies Series). Hoboken, NJ: John Wiley & Sons, Inc., 2021. DOI: 10.1002/9781119332237.

[21] C. Feng, H. Wang, and X. M. T. and, "Geometric mean of nonnegative random variable," *Communications in Statistics - Theory and Methods*, vol. 42, no. 15, pp. 2714–2717, 2013. DOI: 10.1080/03610926.2011.615637. eprint: https://doi.org/10.1080/03610926.2011.615637. [Online]. Available: https://doi.org/10.1080/03610926.2011.615637.

Appendix A

Video Data Extraction Code

```
%% Image Processing for Video Data Extraction
% Read in specified video
videoReader = VideoReader("C:\Users\karao\Desktop\MSc Thesis\ArcVideos\
    Osc007_001_NXA4-S1 Camera.avi");

% Create matrix with all frames from video and time vector
frameIndex = 1;
t = 1;
fr = videoReader.FrameRate;

while hasFrame(videoReader)
    frame = readFrame(videoReader);
    framesMatrix(:, :, :, frameIndex) = frame;
    t(frameIndex) = videoReader.CurrentTime;
    frameIndex = frameIndex + 1;
end

% Populate distance array with every frame
dist = zeros(1, frameIndex - 1);

for i = 1:frameIndex-1

% Binarize frame
testImage = framesMatrix(:,:, :, i);
imageGray = imbinarize(rgb2gray(testImage), 0.95);

% Display
figure(1);
imshow(rgb2gray(testImage))
figure(2)
imshow(imageGray)

% Create boundary boxes around objects; width of box used to find arc
% distance
connected = bwconncomp(imageGray);
stats = regionprops(connected, "BoundingBox");
boundingBoxes = vertcat(stats.BoundingBox);

% Filter extraneous objects (arc will always be in same area)
% Check if bounding box is empty first
    if isempty(boundingBoxes) == 1
        dist(i) = 0;
    else
        selection = (boundingBoxes(:, 3) > 10) & (boundingBoxes(:, 1) <
            300);
        filteredImage = cc2bw(connected, ObjectsToKeep=selection);
        % imshow(filteredImage);            % Check if image filtered
```

```
46
47          connected = bwconncomp(filteredImage);
48          stats = regionprops(filteredImage, "BoundingBox");
49          boundingBoxes = vertcat(stats.BoundingBox);
50
51  % Display bounding boxes
52          figure(3)
53          imshow(filteredImage);
54          hold on
55          for k = 1:size(boundingBoxes,1)
56              rectangle('position',boundingBoxes(k,:),'Edgecolor','g')
57          end
58          hold off
59
60  % Distance value is zero when there is no arc, and thus no bounding box
61          if isempty(boundingBoxes) == 1
62              dist(i) = 0;
63  % Any bounding box in the first five seconds of the video is not from
        the
64  % arc
65          elseif t < 5
66              dist(i) = 0;
67  % The arc is almost always in the bounding box with the largest width
68          else
69              % x = max(boundingBoxes(:, 3))          % Value check
70              dist(i) = max(boundingBoxes(:, 3));
71          end
72      end
73  end
74
75  % For data plotting
76   grid on
77   plot(t.', dist, '-', 'Marker', '.', 'MarkerSize', 20, 'LineWidth', 2)
78   xlabel('Time [s]')
79   ylabel('Distance [mm]')
80   title('Video Osc007 Arc Distance Over Time')
81   grid off
82   fontsize(20,"points")
83
84  % Export data
85  % f = gca;
86  % exportgraphics(f, 'C:\Users\karao\Desktop\MSc Thesis\VideoPlotOsc007.
        png');
87  % writematrix(dist.','C:\Users\karao\Desktop\MSc Thesis\VideoData.xls
        ','Sheet',7)
```

Appendix B

Oscilloscope Filtering and Resizing Code

```
%% Signal Processing for Raw Oscilloscope Data
clear

% Read in oscilloscope data
filename = 'C:\Users\karao\Desktop\MSc Thesis\ArcOscilloscopes\
    fileOsc017Osc026.txt';

opts = detectImportOptions(filename);
M = readmatrix(filename, opts);
A = str2double(strrep(M, ',', '.'));
A(1, :) = [];

% Create vectors of time, current, and voltage from the matrix
timeVector = A(:, 1);
currentVector = A(:, 2);
voltageVector = A(:, 3);

% Butterwoth filter
Fs = 1/(timeVector(2) - timeVector(1)); % Sampling frequency
fc = 500;                               % Cutoff frequency at 500 Hz
[b,a] = butter(4, fc/Fs, 'low');        % Fourth order, low pass
    Butterworth filter

% Filtered signal
voltageFiltered = filter(b,a,voltageVector);
currentFiltered = filter(b,a,currentVector);

% Calculate resistance -- filtered, non-resized
% resistanceFiltered = abs(voltageFiltered./currentFiltered);

% Create spreadsheet of non-resized, filtered data
% writematrix(timeVector,'C:\Users\karao\Desktop\MSc Thesis\
    FullFilteredData.xls','Sheet',1, 'Range', 'A2')
% writematrix(resistanceFiltered,'C:\Users\karao\Desktop\MSc Thesis\
    FullFilteredData.xls','Sheet',1, 'Range', 'B2')
% writematrix(currentFiltered,'C:\Users\karao\Desktop\MSc Thesis\
    FullFilteredData.xls','Sheet',1, 'Range', 'C2')
% writematrix(voltageFiltered,'C:\Users\karao\Desktop\MSc Thesis\
    FullFilteredData.xls','Sheet',1, 'Range', 'D2')

%% Data Vector Resizing/Normalization
% Resizing factor
factor = (length(voltageVector)/(max(timeVector)*500));

```

```
% Normalize signal length to video -- unfiltered data
timeFinal = timeVector(1:factor:end);
voltageFinal = voltageVector(1:factor:end);
currentFinal = currentVector(1:factor:end);

% Normalize signal length to video -- filtered data
timeFinalFiltered = timeVector(1:factor:end);
voltageFinalFiltered = voltageFiltered(1:factor:end);
currentFinalFiltered = currentFiltered(1:factor:end);

% Calculate resistance -- unfiltered
resistanceUnfiltered = abs(voltageFinal./currentFinal);

% Calculate resistance -- filtered
resistanceFinalFiltered = abs(voltageFinalFiltered./
    currentFinalFiltered);

%% Plotting and Data Exporting
% Plot
t = tiledlayout(2,1);
title(t, 'Oscilloscope 026')

% Plot original and resized, filtered current for comparison
nexttile(t)
hold on
plot(timeVector, currentVector, 'LineWidth', 2)                % Non-
    resized non-filtered data
%plot(timeVector, currentFiltered, 'LineWidth', 2)             % Non-
    resized filtered data
plot(timeFinalFiltered, currentFinalFiltered, 'LineWidth', 2)  %
    Resized filtered data
title('Oscilloscope Current')
xlim([0 max(timeVector)])
ylim([min(currentVector)*1.5 max(currentVector)*1.5])
xlabel('Time [s]')
ylabel('Current [A]')
yline(0,'--')
legend('Unfiltered Current', 'Filtered Current')
hold off

% Plot original and resized, filtered voltage for comparison
nexttile(t)
hold on
plot(timeVector, voltageVector, 'LineWidth', 2)        % Non-resized
    non-filtered data
% plot(timeVector, voltageFiltered, 'LineWidth', 2)    % Non-resized
    filtered data
plot(timeFinal, voltageFinalFiltered, 'LineWidth', 2)  % Resized
    filtered data
title('Oscilloscope Voltage')
xlim([0 max(timeVector)])
ylim([min(currentVector)*1.5 max(currentVector)*1.5])
xlabel('Time [s]')
ylabel('Voltage [V]')
yline(0,'--')
legend('Unfiltered Voltage', 'Filtered Voltage', 'Location','northwest'
    )
hold off
fontsize(20,"points")

% Export data
% writematrix(voltageFinalFiltered,'C:\Users\karao\Desktop\MSc Thesis\
    InverseRelations.xlsx','Sheet', '26' , 'Range', 'E2')
```

```
93 % writematrix(currentFinalFiltered,'C:\Users\karao\Desktop\MSc Thesis\
     InverseRelations.xlsx','Sheet','26', 'Range', 'F2')
94 % writematrix(resistanceFinalFiltered,'C:\Users\karao\Desktop\MSc
     Thesis\InverseRelations.xlsx','Sheet','26', 'Range', 'G2')
95 % exportgraphics(t, 'C:\Users\karao\Desktop\MSc Thesis\Arc Plots from
     Oscilloscope Data\OscilloscopePlot026.png');
```

Appendix C

MODELS Code for Power Law Expression Arc Resistance

```
MODEL ARCPOWER
INPUT  I1     -- Input current
OUTPUT Rarc   -- Arc resistance
DATA
       topen  -- Time in which arc begins
VAR    Imin   -- Minimum current
       Rarc   -- Arc resistance
       I      -- Input current - absolute value
       distance -- Arc distance with respect to time
       state
INIT
       Imin := 1e-9
       Rarc:= 0.00001
       state := 0
       distance := 0
       I := 0
ENDINIT
EXEC
IF t > topen THEN
   IF abs(I1) < 1.e-9 THEN
        Rarc := 1.e-9
        state := 1
   ELSE
        state := 0
   ENDIF
   IF state = 0 THEN
       IF abs(I1) < Imin then
          I:=Imin
       ELSE
          I:=abs(I1)
       ENDIF
       distance := 524.7649*(t - topen)
       Rarc := (6.21308*((I)**(-1.041308))-0.002)*distance
   ENDIF
ELSE
   Rarc := 0.00001
ENDIF
ENDEXEC
ENDMODEL
```

Appendix D

MODELS Code for Logarithmic Expression Arc Resistance

```
MODEL ARCLOG
INPUT  I1    -- Input current
OUTPUT Rarc  -- Arc resistance
DATA
       topen
VAR    Imin  -- Minimum current
       Rarc  -- Arc resistance
       I     -- Input current - absolute value
       state
       distance -- Arc distance with respect to time
INIT
       Imin := 1e-9
       Rarc:= 0.00001
       state := 0
       distance := 0
ENDINIT
EXEC
IF t > topen THEN
    IF abs(I1) < 1.e-9 THEN
        Rarc := 1.e-9
        state := 1
    ELSE
        state := 0
    ENDIF
    IF state = 0 THEN
         IF abs(I1) < Imin then
          I:=Imin
         ELSE
          I:=abs(I1)
         ENDIF
          distance := 524.7649*(t - topen)
          Rarc:=(-0.02073*log10(I)+0.066)*distance
    ENDIF
ELSE
    Rarc := 0.00001
ENDIF
ENDEXEC
ENDMODEL
```

Appendix E

Test and Simulation Data Comparison Code

```
filename = 'C:\Users\karao\Desktop\MSc Thesis\InverseRelations.xlsx';
M = readmatrix(filename,'Sheet','Sheet1','Range','E3:G415');

t = 0:0.0001:0.824;
time = 0:0.002:0.824;

% Real test values
voltage = M(:, 1);
current = M(:, 2);
resistances = M(:, 3);

% ATP calculated values
current_atp = iArcvolXx0004;
Rarc_atp = mRarc;
Uarc_atp = vArcvol;

% Voltage Comparison Plot
figure(1)
plot(time, voltage, 'LineWidth', 2)
hold on
plot(t, Uarc_atp, 'LineWidth', 2)
hold off
xlabel('Time [s]')
ylim([-8000, 8000])
ylabel('Voltage [V]')
legend('Test Data Voltage', 'ATP Calculated Voltage')
title('Voltage Comparison')
fontsize(20,"points")

% Current Comparison Plot
figure(2)
plot(time, -current, 'LineWidth', 2)
hold on
plot(t, current_atp, 'LineWidth', 2)
hold off
xlabel('Time [s]')
ylabel('Current [A]')
ylim([-8000, 8000])
legend('Test Data Current', 'ATP Current')
title('Current Comparison')
fontsize(20,"points")

% Resistance Comparison Plot
figure(3)
```

```
45 plot(time, resistances, 'LineWidth', 2)
46 hold on
47 plot(t, Rarc_atp, 'LineWidth', 2)
48 hold off
49 legend('Test␣Data␣Resistances', 'ATP␣Calculated␣Resistances')
50 ylim([0 10])
51 xlabel('Time␣[s]')
52 ylabel('Resistance␣[\Omega]')
53 title('Resistance␣Comparison')
54 fontsize(20,"points")
```